

Modulation of equatorial Pacific westerly/easterly wind events by the Madden–Julian oscillation and convectively-coupled Rossby waves

Martin Puy¹ · J. Vialard¹ · M. Lengaigne^{1,2} · E. Guilyardi^{1,3}

Received: 2 December 2014 / Accepted: 30 May 2015 / Published online: 16 June 2015
© Springer-Verlag Berlin Heidelberg 2015

Abstract Synoptic wind events in the equatorial Pacific strongly influence the El Niño/Southern Oscillation (ENSO) evolution. This paper characterizes the spatio-temporal distribution of Easterly (EWEs) and Westerly Wind Events (WWEs) and quantifies their relationship with intra-seasonal and interannual large-scale climate variability. We unambiguously demonstrate that the Madden–Julian Oscillation (MJO) and Convectively-coupled Rossby Waves (CRW) modulate both WWEs and EWEs occurrence probability. 86 % of WWEs occur within convective MJO and/or CRW phases and 83 % of EWEs occur within the suppressed phase of MJO and/or CRW. 41 % of WWEs and 26 % of EWEs are in particular associated with the combined occurrence of a CRW/MJO, far more than what would be expected from a random distribution (3 %). Wind events embedded within MJO phases also have a stronger impact on the ocean, due to a tendency to have a larger amplitude, zonal extent and longer duration. These findings are robust irrespective of the wind events and MJO/CRW detection methods. While WWEs and EWEs behave rather symmetrically with respect to MJO/CRW activity, the impact of ENSO on wind events is asymmetrical. The WWEs occurrence probability indeed increases when the warm pool is displaced eastward during El Niño events, an increase that can partly be related to interannual modulation of the MJO/CRW activity in the western Pacific. On

the other hand, the EWEs modulation by ENSO is less robust, and strongly depends on the wind event detection method. The consequences of these results for ENSO predictability are discussed.

Keywords Westerly wind events · Easterly wind events · ENSO · Madden–Julian Oscillation · Convectively-coupled Rossby waves

1 Introduction

The El Niño Southern Oscillation (ENSO) is the dominant mode of interannual climate variability at the global scale. ENSO's trademark anomalies are anomalously warm Sea Surface Temperatures (SSTs) and anomalously weak easterlies in the central and eastern equatorial Pacific. El Niño has worldwide impacts (e.g. McPhaden et al. 2006a) through teleconnections between equatorial Pacific temperature and the global atmospheric circulation (Trenberth et al. 1998). Because of its socio-economic consequences, modelling and forecasting ENSO is of crucial importance and remains a key challenge (Barnston et al. 2012; Vecchi and Wittenberg 2010; Guilyardi et al. 2012).

The critical mechanism for ENSO's growth is an unstable air–sea interaction between SST anomalies in the central Pacific and the strength of the Walker circulation, known as the positive Bjerknes feedback (Bjerknes 1969). One widely accepted mechanism for the delayed negative feedback that terminates an ENSO was formulated in the framework of the “recharge oscillator” theory (Jin 1997), where El Niño wind anomalies drive a Sverdrup transport out of the equatorial strip, which raise the average level of the equatorial thermocline and favour a switch towards La Niña conditions. In this framework, the upper

✉ Martin Puy
Martin.Puy@locean-ipsl.upmc.fr

¹ LOCEAN/IPSL, Sorbonne Universités, UPMC, Univ Paris 06-CNRS-IRD-MNHN, Paris, France

² Indo-French Cell for Water Sciences, IISc-NIO-IITM-IRD Joint International Laboratory, NIO, Goa, India

³ NCAS-Climate, University of Reading, Reading, UK

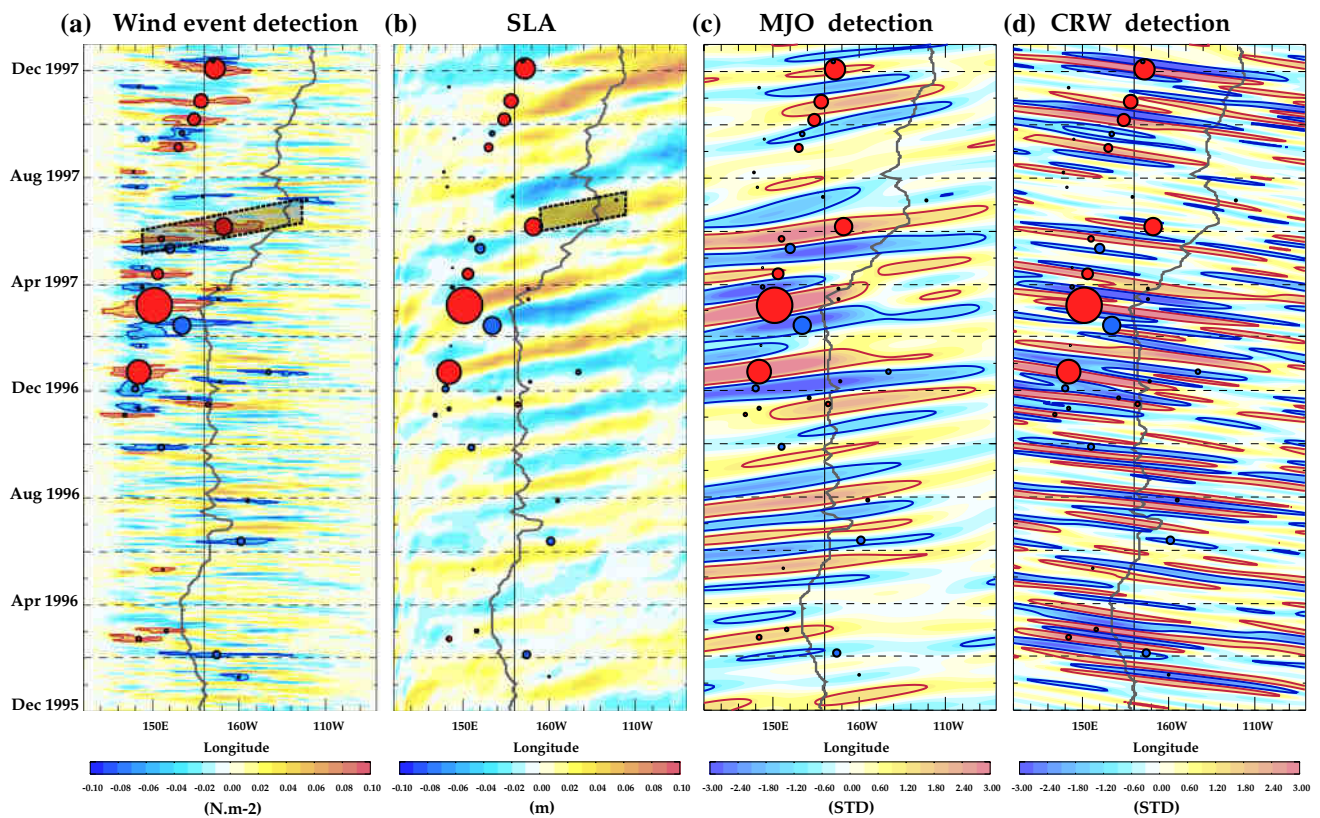


Fig. 1 Averaged 2°N – 2°S time-longitude section of **a** intraseasonal zonal wind stress, **b** intraseasonal sea level anomalies, **c** MJO-related wind stress signal with detected convective (*red contour*) and suppressed (*blue contour*) MJO phases overlaid and **d** CRW-related wind stress signal with convective (*red contours*) and suppressed (*blue contours*) CRW phases overlaid, before and during the 1997 El Niño. The *black contour* on all panels indicates the eastern edge of the western Pacific Warm Pool (defined as the 28.5°C isotherm). *Red* and *blue circles* respectively indicate the detected WEs and

EWEs central dates and longitudes, the size of the circle being proportional to WEs/EWEs strength depicted as the non-dimensional Wind Event Index (see Sect. 3.1 for details). The *dotted black box* on (a) indicates the spatio-temporal domain over which SLA response shown in Fig. 3a, b is averaged (see text for details). The *dotted black box* on (b) indicates the spatio-temporal domain over which wind stress forcing along the wave track used in Fig. 3b is averaged (see text for details). Note that the strong December 1996 and March 1997 WEs were both associated with a convective MJO and CRW

ocean equatorial heat content is a robust El Niño precursor (Meinen and McPhaden 2000). Aside this precursor, other factors are however required to explain the irregularity of ENSO. A large body of literature suggested that high-frequency wind variability could play an important role in ENSO dynamics and predictability (Kleeman and Moore 1999; Zavala-Garay et al. 2005; McPhaden et al. 2006b; Shi et al. 2009; Wang et al. 2011). A large part of this high-frequency forcing occurs in the form of Westerly Wind Events (WWEs), characterized as episodes of anomalous, short-lived, but strong westerlies developing over the western Pacific warm pool (e.g. Luther et al. 1983; Lengaigne et al. 2004a). These WWEs promote the onset and/or development of El Niño events (Fedorov 2002; Boulanger et al. 2004; Lengaigne et al. 2004b) and to contribute to the irregularity of ENSO, in terms of timing (its broad spectrum ranging between 2 and 7 years; e.g. Gebbie et al.

2007; Jin et al. 2007), magnitude (Eisenman et al. 2005; Gebbie et al. 2007) and spatial patterns (Fedorov et al. 2015; Hu et al. 2014; Lian et al. 2014).

Because of their role in ENSO dynamics, several studies have offered detailed descriptions of the wind field evolution during individual WWEs (Chang et al. 1979; Chen and Houze 1997; Eldin et al. 1994; Keen 1982; Lin and Johnson 1996; Love 1985) or of the statistics of WWEs characteristics based on a larger number of events (Harrison and Giese 1991; Hartten 1996; Harrison and Vecchi 1997; Verbickas 1998; Fasullo and Webster 2000; Seiki and Takayabu 2007a, b). These studies show that WWEs are generally associated with enhanced clouds and precipitation and preferentially occur over the western Pacific warm pool during boreal winter and spring. They typically have a 20–40 degrees zonal extent, 5–10 degrees meridional scale, 5–30 days duration and $5\text{--}7\text{ m s}^{-1}$ amplitude.

The oceanic response to WWEs is illustrated on Fig. 1a, b for the case of a series of well documented WWEs (McPhaden and Yu 1999; McPhaden 1999; Yu and Rienecker 1998; van Oldenborgh 2000; Bergman et al. 2001; Lengaigne et al. 2002, 2003, 2004b; Boulanger et al. 2001, 2004; Menkes et al. 2014), which occurred prior and during the development of the 1997/98 El Niño event, the strongest on record. Most WWEs (red circles on Fig. 1a) drive eastward anomalous currents and an anomalously deep thermocline signals (Fig. 1b), both locally under the wind perturbation and further eastward along the Kelvin downwelling wave path (Boulanger and Menkes 1999; McPhaden 2002). The most intense WWE in this series occurred in March 1997 (Fig. 1a) and was followed by a rapid eastward displacement of the Western Pacific Warm Pool Eastern Edge (hereafter, WPEE, black solid line on Fig. 1), that has been attributed to zonal advection by anomalous eastward current (Boulanger et al. 2001; Lengaigne et al. 2002; Chiodi et al. 2014).

While WWEs are synoptic events that are unpredictable at long lead times, there is a growing body of observational evidence showing that their probability of occurrence is modulated by low-frequency SST variability, with more likely WWEs prior to and during most El Niño events (e.g., Keen 1982; Luther et al. 1983; Delcroix et al. 1993; Verbickas 1998; Vecchi and Harrison 2000; Seiki and Takayabu 2007a), i.e. when the warm pool is anomalously extended eastward (Eisenman et al. 2005; Gebbie et al. 2007). Modelling studies support these observational findings and show that eastward displacement of the WPEE favours the WWEs occurrence (Lengaigne et al. 2003; Vecchi et al. 2006). This air–sea coupled dynamical process, in which the WWE-driven eastward expansion of the WPEE enhances the probability of further WWEs occurrence, could partly explain the diversity of ENSO characteristics (Eisenman et al. 2005; Tziperman and Yu 2007; Jin et al. 2007; Gebbie and Tziperman 2009a, b).

WWEs basic characteristics and their relationship with tropical Pacific background SST are well documented but their root causes are still debated. An important fraction of intraseasonal wind and convective variability over the western Pacific warm-pool is controlled by the Madden–Julian Oscillation (Madden and Julian, 1971, 1972, 1994), making it a serious candidate for WWEs modulation. The MJO is the dominant source of intraseasonal (30–90 days) atmospheric variability in the tropical Indo-Pacific region. This tropic-wide phenomenon is associated with large-scale variations in wind and atmospheric convection (wave number 1 and 2), which propagate eastward with an average speed of 5 m s^{-1} . The clearest MJO surface signature occurs over warm SSTs that sustain deep atmospheric convection ($\text{SST} > 28.5 \text{ }^\circ\text{C}$, e.g. Gadgil et al. 1984), i.e. in the Indo-Pacific warm pool region, and near the Pacific

Intertropical and South Pacific Convergence Zones (Zhang 2005). In the lower troposphere, the convective phase of the MJO is associated with anomalous westerly winds in and to the west of the large-scale convective centre, and anomalous easterly winds to the east. Previous studies have shown that the MJO activity also shift eastwards into the central Pacific as El Niño develops (e.g., Hendon et al. 1999; Bergman et al. 2001; Kessler 2001; Zhang and Gottschalck 2002; McPhaden et al. 2006b). This expansion can largely be related to the eastward expansion of the warm pool before El Niño events, which allows the MJO to express its surface signature over a larger zonal fetch (Kessler 2001). Some studies have also explored how the MJO may influence ENSO (e.g. Kessler et al. 1995; Kessler and Kleeman 2000; Roulston and Neelin 2000; Zavala-Garay et al. 2005). This is not obvious as the MJO is generally thought to have a symmetric signal in surface forcing, which may not result in a mean oceanic response over a MJO cycle. Kessler et al. (1995) however proposed that the eastward expansion of the warm pool during convective phases of the MJO allows westerly wind anomalies to act over a larger zonal fetch than during the suppressed phase, providing an asymmetry that could produce a non-zero effect of the MJO over one cycle. Kessler and Kleeman (2000) alternatively show that the net evaporative cooling of SST, produced by high wind speeds associated with oscillating winds on a weak mean flow, results in a flattening of the background zonal SST gradient that may result in a stronger ENSO.

Contrary to the MJO, WWEs are associated to a mean westerly wind anomaly that can contribute to ENSO growth in a more obvious way. An obvious way by which the MJO could influence ENSO is thus through WWEs modulation. Many studies did suggest that the MJO indeed modulates the intensity and frequency of WWEs over the western Pacific warm waters (Lau et al. 1989; Gutzler 1991; Sui and Lau 1992; Zhang 1996; Lin and Johnson 1996; Chen et al. 1996; Godfrey et al. 1998; McPhaden 1999). The series of strong WWEs that occurred from December 1996 to July 1997 (Fig. 1a) has for instance been attributed to the convective phases of a series of unusually strong MJO events (Fig. 1c, Yu and Rienecker 1998). The statistical relationship between WWEs and the MJO is however still debated: the only two studies that did assess thoroughly this relationship over a long period and a large set of WWEs indeed disagree (Seiki and Takayabu 2007a; Chiodi et al. 2014). Both studies acknowledge that WWEs are more likely to occur during an MJO convective phase rather than during its suppressed phase. Chiodi et al. (2014) concluded that the probability of a WWE occurrence remain the same irrespective of whether the MJO is active or not (an MJO active period being defined as the envelope of successive convective and suppressed phases, see Fig. 2b for a sketch explaining the terminology that we use in this

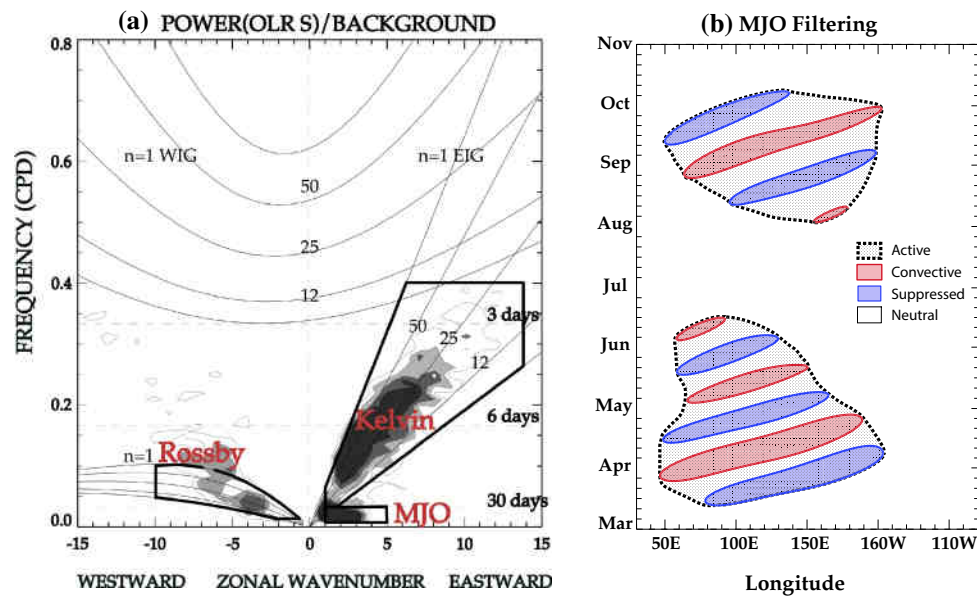


Fig. 2 **a** Wavenumber-Frequency spectrum of the symmetric part of the OLR at the equator, as in Wheeler and Kiladis (1999). The *black boxes* highlight the wavenumber-frequency filtering used for isolating the Kelvin, Rossby waves and the MJO. **b** Sketch illustrating the terminology used for designating the MJO and Rossby waves various phases throughout the paper. This example is derived from the MJO index (defined in Sect. 2.3) between March and November 2005. “Convective” phases (*red lines*) are defined as index values exceeding one standard deviation. “Suppressed” phases (*blue lines*)

are defined as index values below minus one standard deviation. “Active” phases (*dotted lines*) are defined as the envelope of a series of closely-occurring convective and suppressed phases. Periods within an active period that are neither convective nor suppressed are referred as “transition” periods. Finally, periods in *white* are referred as “neutral” phases. The example above is provided for the MJO, but Rossby waves display similar “active” phases that contain both convective, suppressed and transition periods

paper). In contrast, Seiki and Takayabu (2007a) results suggest that large-amplitude active MJO periods are especially conducive to WWEs. These later results echo those of Fasullo and Webster (2000) who suggested that brief WWEs (6–30 days) occur frequently, independently of the MJO, while sustained WWEs are strongly associated with the MJO convective phase. The reason behind the disagreement between Seiki and Takayabu (2007a) and Chiodi et al. (2014) results remain to date unravelled.

The root cause for convective blow-ups and WWEs over Pacific warm waters has not only been attributed to MJO events but also to the occurrence of twin or individual tropical cyclones (Keen 1982; Love 1985; Nitta 1989; Lander 1990). The majority (>60 %) of the WWEs that are west of the dateline are in fact related to cyclonic vortices (Harrison and Vecchi 2001), and the strongest, longer lasting, and more horizontally extended WWEs are often those related to symmetrical pair of cyclones with respect to the equator (Harrison and Giese 1991; Hartten 1996). These cyclones pairs often appear as the result of atmospheric Convectively-coupled Rossby Waves (hereafter CRW) as suggested by Seiki and Takayabu (2007a). CRW result from the coupling between atmospheric convection and equatorial waveguide dynamics, and are characterized by periods of 15–20 days and westward propagating signals at about

5–7 m s^{-1} (Wheeler and Kiladis 1999; Yang et al. 2007). The convective phase of CRW is associated with anomalous westerly winds at the equator with maximum amplitude over the Indian Ocean and western Pacific in boreal spring. CRW and the MJO are not completely independent, as CRW are often dynamically part of the MJO life cycle (e.g. Rui and Wang 1990). The composite analysis of Seiki and Takayabu (2007a) show that intensified Rossby wave activity with symmetrical cyclone like vortices on each side of the equator is a common feature associated with WWEs occurrence, but this study did however not quantify the percentage of WWEs associated with such CRW.

While most studies have so far focussed on WWEs and their impact on ENSO, a recent study (Chiodi and Harrison 2015) underlined that counterparts to WWEs exist as surges in the easterly wind stress. These events, referred to as Easterly Wind Events (EWEs) in the following, have an average duration, amplitude and zonal extent roughly similar to those of WWEs. The blue circle in February 1997 on Fig. 1a indeed illustrates the occurrence of a moderate EWE. Chiodi and Harrison (2015) suggest that, symmetrical to the impact of WWEs on El Niño, EWEs may contribute to cold tongue cooling during La Niña events. Along the same line, Lengaigne et al. (2006) suggested that central Pacific EWEs can contribute to warm events

termination and reversal into neutral or La Niña conditions. Boulanger et al. (2004) also underlined that high-frequency easterly wind pulses contributed to the amplitude and timing of the 1997–1998 warm event. Finally, Chiodi and Harrison (2015) suggest that, as WWEs, EWEs vary with ENSO state, with an increase probability of EWEs occurrence during cold conditions. EWEs have however so far received less attention than their westerly counterparts and their relationship with atmospheric phenomena such as MJO and CRW have not yet been investigated.

Owing to the potential importance of WWEs and EWEs on the tropical Pacific evolution, there is a need to better identify the main processes that modulate their occurrence in order to ultimately improve their prediction. As detailed above, the relationship between wind events and atmospheric phenomena such as MJO/CRW remain controversial or elusive. The present paper aims at providing a clearer picture of the relationship between these short-lived wind events and the MJO, CRW and background SST. The datasets and methods used to define the wind events (EWEs and WWEs) and atmospheric waves (MJO and CRW) are described in Sect. 2. Section 3 then assesses the main characteristics (amplitude, seasonality, location) of these detected events and proposes a new index to describe their potential impact on the ocean. In Sect. 4, we demonstrate a clear modulation of wind events by both the MJO and CRW, which is quite symmetric for EWEs and WWEs. We also demonstrate the robustness of our results, by varying detection thresholds and methods for both wind events and atmospheric wave. In Sect. 5, we evaluate the relationship between WWEs/EWEs and interannual background SST variability. We find that WWEs probability increases during El Niño events, in agreement with previous studies. The effect of interannual variability on EWEs is however not robust with respect to the wind event detection method, indicating a more asymmetric effect of interannual than of intraseasonal variability on wind events. A discussion of

the present findings in the light of previous studies and of their potential implications is finally provided in Sect. 6.

2 Datasets and methods

2.1 Datasets

We use TropFlux daily zonal wind stresses (Praveen Kumar et al. 2012, <http://www.incois.gov.in/tropflux/>) on a $1^\circ \times 1^\circ$ degree grid over the 1979–2014 period to detect WWEs and EWEs. TropFlux wind stresses are computed using the COARE v3.0 algorithm, using bias and amplitude-corrected ERA-Interim surface meteorological data (Dee et al. 2011). A comparison between the TropFlux product and in situ observations (TAO moorings) indicates that this product is amongst the best at intraseasonal timescales, with correlations above 0.95 in the equatorial western and central Pacific. We also use the NOAA daily-interpolated OLR from January 1974 to December 2013 (http://www.esrl.noaa.gov/psd/data/gridded/data.interp_OLR.html) to describe deep atmospheric convective signals associated with these wind events and TropFlux SST to describe the background SST conditions. Finally, we use weekly sea level anomaly from AVISO with a $1/4^\circ \times 1/4^\circ$ spatial resolution from 1992 to 2014 (<http://www.aviso.oceanobs.com/en/data/products/>) in order to assess their oceanic signature.

2.2 Wind events detection method

Several authors have developed WWEs detection algorithms in the past, using various criteria (Hartten 1996; Harrison and Vecchi 1997; Seiki and Takayabu 2007a). Those criteria and methods are summarized in Table 1. In the present paper, we are interested by wind events that are likely to have a significant oceanic impact. We will therefore focus on events that have an equatorial signature, as

Table 1 Different methods used to detect westerly wind events in the literature

Studies	Hartten (1996)	Harrison and Vecchi (1997)	Seiki and Takayabu (2007a)	Chiodi et al. (2014)	Current study
Field	1000 mbar zonal wind	10 m wind	10 m wind	10 m wind	Zonal wind stress
Product	ECMWF/WMO	ECMWF analysis	ERA-40	ECMWF analysis	Tropflux
Filtering (anomaly)	Raw field	Relative to seasonal cycle	Relative to seasonal cycle	Relative to seasonal cycle	Intraseasonal (5–90 days)
Period	1980–1989	1986–1995	1979–2002	1986–2010	1979–2012
Min duration	2 days	3 days	2 days	3 days	5 days
Min Zonal extent	10°	Averaged in 30° boxes	10°	Averaged in 30° boxes	10°
Min magnitude	5 m s^{-1}	2 m s^{-1}	5 m s^{-1}	2 m s^{-1}	0.04 N m^{-2}
# of detected WWEs	~15/years	~16/years	~8/years	~11/years	~6/years

only these events are likely to force equatorial waves. We will use wind stress rather than wind speed for their detection because wind stress is a direct measure of the surface momentum flux and wind speed is non-linearly related to it. Another difference with previous studies is that wind events are identified from intraseasonally filtered (5–90 day) wind stresses rather than absolute winds (e.g., Hartten 1996, Table 1) or anomalies relative to the seasonal cycle (e.g., Harrison and Vecchi 1997; Seiki and Takayabu 2007a, Table 1). We will discuss how this choice may affect our results in Sect. 5. Our motivation for using intraseasonally filtered wind stresses is twofold. First, at timescales longer than ~90 days (i.e. the time it takes for a Kelvin wave to cross the basin), there tends to be a balance between zonal wind stress and zonal pressure gradients (McPhaden and Taft 1988; Yu and McPhaden 1999). Our filtering strategy is therefore motivated by the fact that we are mostly interested in shorter variations that will induce a disequilibrium between the two and an ocean response. Second, using raw winds or even interannual anomalies will computationally induce more WWEs (EWEs) detection during El Niño (La Niña) events when there are low-frequency westerly (easterly) wind anomalies. We will hence be able to evaluate if the tendency to have more WWEs before/during ENSO underlined in previous studies from a detection method using interannual anomalies is still observed if wind events are detected on the basis of intraseasonally filtered wind stresses.

As in most previous studies (Hartten 1996; Harrison and Vecchi 1997; Seiki and Takayabu 2007a; Chiodi et al. 2014, Table 1), our detection method is based on three thresholds: zonal extension, duration and magnitude of the wind event. Previously used magnitude thresholds criteria range from 2 m s⁻¹ (Harrison and Vecchi 1997) to 5 m s⁻¹ (Hartten 1996; Seiki and Takayabu 2007a). A 5 m s⁻¹ wind corresponds to a wind stress of ~ 0.03 N m⁻² in an atmosphere with neutral stability (Trenberth et al. 1989). The minimum duration criteria range from 2 (Hartten 1996; Seiki and Takayabu 2007a) to 3 days (Harrison and Vecchi 1997; Chiodi et al. 2014) and the zonal extend is usually taken as 10°. We decided to use conservative criteria (i.e. rather strong, long-lasting wind events with a large zonal extent) to focus on events that are likely to significantly impact the ocean evolution. The WWE (resp. EWE) are hence defined as 2°N–2°S averaged intraseasonal (5–90 days) wind stress anomalies above 0.04 N m⁻² (resp. below -0.04 N m⁻²) with a zonal extent of at least 10° during at least 5 days. The standard deviation of the 2°N–2°S averaged zonal wind stress anomalies is 0.036 N m⁻², indicating that the first criterion roughly picks up wind stress anomalies larger than one standard deviation. Finally, a last criterion is used to merge wind events that are close in space or time: wind stress anomalies patches satisfying the duration, zonal

extent and magnitude criteria, separated by less than 3 days and 3° are considered to be a single wind event. The central location lon0 and date day0 for each wind event are computed using a weighted average as follows:

$$lon0 = \frac{\int_x \int_t lon(x) \cdot \tau_x(x, t)}{\int_x \int_t \tau_x(x, t)}$$

$$day0 = \frac{\int_x \int_t time(t) \cdot \tau_x(x, t)}{\int_x \int_t \tau_x(x, t)}$$

where τ_x is the zonal wind stress intraseasonal anomaly and the space and time integrals are computed over the spatio-temporal domain of the wind stress patch.

Using this method, we identify 208 WWEs and 197 EWEs over the 1979–2014 period, corresponding to ~6 WWEs and ~6 EWEs per year. This is less than what was found in Harrison and Vecchi (1997) (~16 WWEs/years) and Seiki and Takayabu (2007a) (~8 WWEs/years). These differences are mainly due to our more restrictive magnitude criteria that only pick up strong events. The sensitivity of our results to the WWE detection method will be extensively discussed in Sect. 4.2.2.

2.3 Atmospheric intraseasonal waves detection method

The different atmospheric convectively coupled waves components are obtained following Wheeler and Kiladis (1999). This method is illustrated by the wavenumber-frequency spectrum of the symmetric part of the OLR at the equator displayed on Fig. 2a. This figure demonstrates that energy preferentially appears along the dispersion diagram of equatorially trapped waves, with eastward phase propagation at ~10–15 m s⁻¹ for convectively coupled Kelvin waves and westward phase propagation at ~-7 m s⁻¹ for the first baroclinic convectively coupled Rossby waves. The MJO appears as an extra patch of energy with large spatial scales (wavenumbers 1–5) and eastward propagation at ~5 m s⁻¹. As in Wheeler and Kiladis (1999), the MJO is defined by space–time filtering in the domain outlined on Fig. 2a (westward-propagating wavenumber 1–5, 30–95 days band). The wavenumber-frequency boundaries used for isolating the convectively coupled Kelvin and Rossby waves (or CRW) correspond to the theoretical dispersion curves for the 8 and 90 m equivalent depths, also depicted on Fig. 2a.

Below, we will focus on MJO and CRW identification, as we could not find any relationship between wind events and convectively coupled Kelvin waves (not shown). The space–time filtering described above is applied to

equatorial zonal wind stress to isolate its CRW and MJO components. The resulting fields are normalized by their standard deviation computed between 130°E to 160°W, corresponding to the region where 90 % of the WWEs and EWEs are detected. The resulting standardized MJO and CRW related zonal wind stress components are shown on Fig. 1c, d for the 1996–1997 period. Regions above one standard deviation are considered as convective phases (red contours on Fig. 1c, d, also see sketch on Fig. 2b) while regions below minus one standard deviation are considered as suppressed phases (blue contours on Figs. 1c, d and 2b). An “active” period is finally defined as the envelope of successive convective and suppressed phases (Fig. 2b), and considered to end when a transition phase is longer than 30 days. We will finally refer to intervals within active periods that are neither convective nor suppressed as “transition” phases (Fig. 2b). Using these criteria, about 161 (358) convective phases of MJO (CRW) are identified over the 1979–2013 period, spanning ~16 % of the total period. As shown on Fig. 1c and discussed in the introduction, the strongest MJO activity on record occurred in association with a series of intense WWEs from December 1996 to July 1997 in the western Pacific. This period was also characterized by enhanced CRW activity in the central Pacific. We will assess if the modulation of wind events by the MJO and CRW suggested by Fig. 1 exists over the entire period in Sect. 4, which will also discuss the sensitivity of our results to the definition of MJO and CRW phases.

3 Wind events main characteristics

This section first describes a metric that allows estimating the amplitude of the oceanic response to a wind event and then discusses the main characteristics of the amplitude, seasonal and spatial distribution of WWEs and of EWEs.

3.1 An index to characterize the wind events oceanic impact

Wind events force several distinct oceanic responses. Locally, they induce evaporative cooling which deepens and cools the mixed layer (e.g. McPhaden 2002). They also force eastward propagating Kelvin waves and westward propagating Rossby waves that are associated with thermocline depth modulation and current anomalies (e.g. Boulanger and Menkes 1999). At the eastern edge of the warm pool, both lateral advection and surface heat fluxes contribute to SST changes, while the SST change is dominated by vertical processes (changes in upwelling and mixing) further east, due to the shallower background thermocline depth (e.g. Drushka et al. 2015). While the local and remote SST response can vary substantially due to the changes in

background oceanic situations (e.g. zonal SST gradient), the Kelvin wave response to the wind event is more robust. Since this Kelvin wave is generally responsible for a large part of the SST changes both in the central (through lateral advection) and eastern (through vertical processes) Pacific, we will use its sea level responses as an index to characterize the ocean response to wind event forcing.

Linear equatorial wave theory provides a framework to understand the equatorial ocean response to wind stress forcing. The oceanic response is expected to grow with the intensity of the forcing (i.e. the wind stress anomaly magnitude), its duration and its zonal fetch (e.g. a larger zonal patch will influence a Kelvin wave over a longer portion along its path; see Giese and Harrison 1990). An integration of the wind events anomalies along the equatorial waves path would allow to precisely estimate their oceanic impact. Here, we chose a simpler “wind event index” (WEI) to characterize the response of the ocean to a Wind event. We define the WEI as the space–time integration of the zonal wind stress anomalies over the wind event patch $\int \int \tau_x(x, t).dx.dt$. The WEI definition hence integrates the wind event amplitude, duration and zonal fetch. Once computed for all wind events (both easterly and westerly), the WEI is normalized by its standard deviation to obtain a dimensionless index.

Sea level is a precise measure of the amplitude of the depth-integrated oceanic response to a wind event. Figure 1b illustrates the sea level anomalies during the onset of the 1997–1998 El Niño, with strong downwelling Kelvin waves in response to the intense WWEs occurring in December 1996 and March 1997 and an upwelling Kelvin wave response to the EWE in February 1997. Figure 3 demonstrates the ability of the WEI to efficiently capture the amplitude of the Kelvin wave response to the wind event. The Kelvin wave response to wind events is estimated as the average 5–90 day-filtered sea level anomalies along the Kelvin wave path, i.e. within a space time-domain starting at lon0, day0 and extending for 20 days in time and up to 40° eastward in space and using a theoretical speed of 2.5 m s⁻¹ (an example of the integration domain is showed on Fig. 1b). The scatterplot between the WEI of each detected wind event and this Kelvin wave response displayed on Fig. 3a demonstrates a tight connection between these two indices, with a 0.76 correlation between the SLA response to a wind event and the WEI, significant at 95 % (using one-tail *t* test with a effective degrees of freedom estimated as in Livezey and Chen 1983). This strong correlation indicates that the WEI is a reliable measure of oceanic response to the wind event. Figure 3b shows that the spread on Fig. 3a largely arises from the additional wind forcing along the Kelvin wave path, that contributes to the sea level signal both up- and down-stream of the wind event. This additional forcing is calculated here as

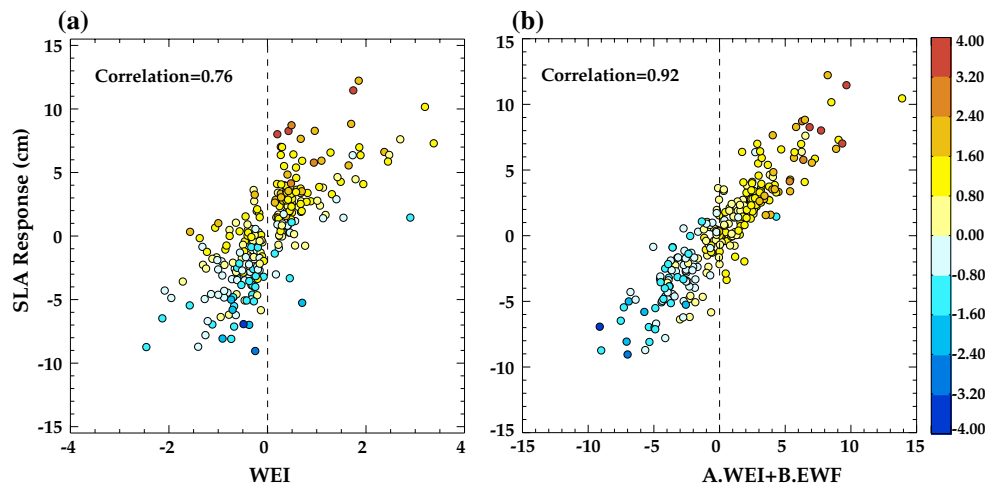


Fig. 3 **a** Scatter diagram of the Wind Event Index (WEI, i.e. the normalized space–time integral of the average 2°N – 2°S zonal wind stress anomaly over the wind event patch; see text for details) against the observed mean sea level anomaly averaged along the Kelvin wave path downstream of the wind event (see text for details). Positive WEI values indicate WWEs while the negative ones indicate EWEs. The *color* of each *dot* represents the integrated wind forcing (excluding

the wind event) along the Kelvin wave track (see text for details). **b** Scatter diagram of a linear combination of the normalized WEI and forcing along the wave track (obtained from a multiple linear regression, with roughly equal contributions from each) and observed mean sea level anomaly averaged along the Kelvin wave path downstream of the wind event

the zonal wind stress anomalies (excluding the wind event anomalies) averaged along the Kelvin wave path theoretical speed (2.5 m s^{-1}) between 10 days prior and 10 days after the wind event (corresponding to 40° in longitude; an example of the integration domain is showed on Fig. 1a). A multi-linear fit of the SLA response to the WEI and this additional forcing results in a 0.92 correlation significant at the 95 % (Fig. 3b). This analysis hence confirms that the WEI can be used as a proxy for the strength of ocean response to the wind event, but indicates that forcing along the Kelvin wave path outside of the wind event patch also contributes to the sea level response.

3.2 Wind events characteristics and distribution

In this section, we assess the spatio-temporal characteristics of WWEs and EWEs detected by our method and briefly compare our results to the existing literature on that topic.

Figure 4 first allows discussing the average wind event spatio-temporal structure. The first column of the Fig. 4 displays five composite maps of intraseasonal OLR and wind stress (5–90 days) anomalies centred on the WWEs central date and longitude from 8 days prior to 8 days after the events central date. At day0, WWEs are characterized by westerly wind stress anomalies with a 30° zonal extent, associated with a rather symmetrical convective pattern with respect to the equator. Composite maps at different lags indicate an eastward propagation of the suppressed convection region, at a speed of around $5\text{--}7 \text{ m s}^{-1}$, consistent with MJO characteristics. It also confirms that a pair of

cyclonic wind stress anomalies centred around 10°N and 10°S is a common feature associated with WWEs. This symmetric pair of cyclones is reminiscent of the equatorial Rossby wave structure as confirmed by the westward propagation of these anomalies for day0 to day+8 north of the equator. Seiki and Takayabu (2007a) already noted these features in their composite analysis (their Fig. 10) and did suggest that they resulted from the tendency of WWEs to occur during convective phases of MJO and CRW.

The second column of Fig. 4 displays similar composite maps for EWEs. EWEs display roughly symmetrical anomalies to those associated with WWEs and lagged composite maps also suggest a modest eastward propagation of convective anomalies, reminiscent of the MJO signature. The main differences with the WWEs composites arise from the smaller amplitude OLR and wind stress perturbations with a larger zonal extension at day0 (50 degrees) and a weaker Rossby wave signal on both side of the equator.

Figure 5 provides a quantitative assessment of the wind events distribution. Figure 5a shows that WWEs tend to be more frequent in boreal winter and less frequent from May to October. 90 % of WWEs occur in the western Pacific, west of the dateline (Fig. 5b). Despite differences in the wind event detection method, these results are consistent with those of Keen (1982), Harrison and Vecchi (1997) and Seiki and Takayabu (2007a), an indication of their robustness. The WEI distribution of these WWEs (Fig. 5c) is not normal, with an enhanced probability of wind events with weak or very strong WEI (WEIs below 1 or above 2). EWEs are more likely to occur in boreal winter and less

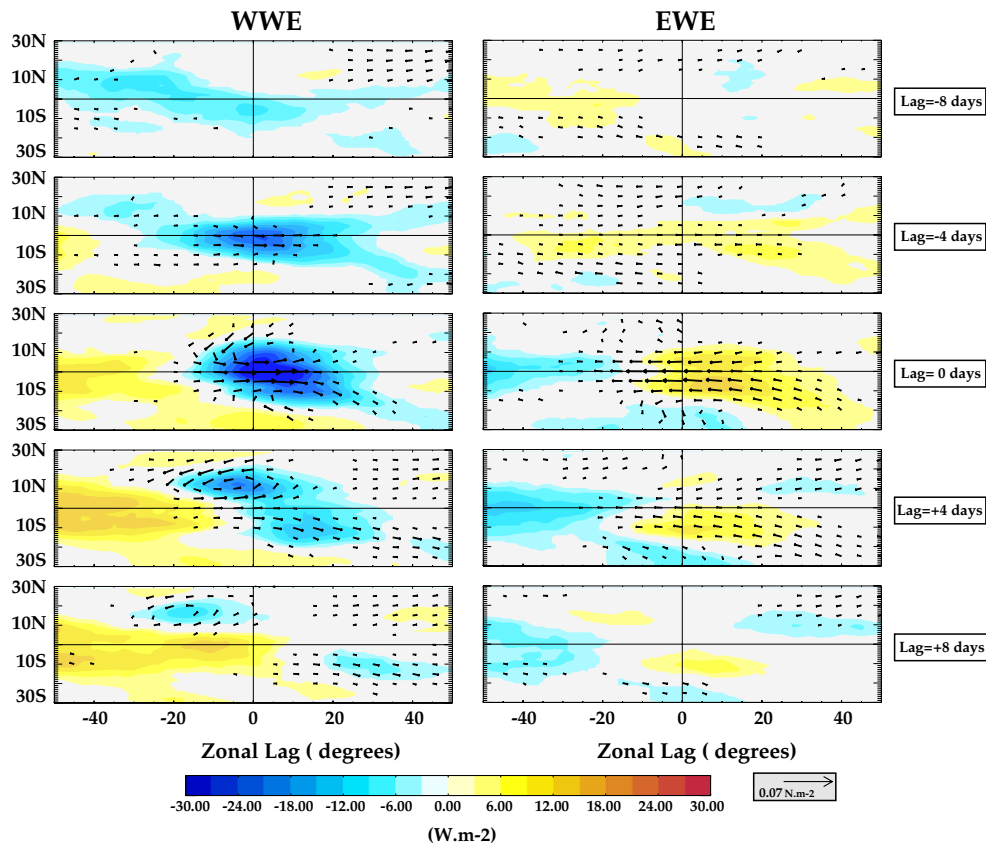


Fig. 4 Spatial composite of (left) WWEs and (right) EWEs intraseasonal wind stress (vectors) and OLR (shading) anomalies from 8 days prior to 8 days after the wind event. The composites are centred on central dates and longitudes of the wind event

likely in boreal summer (Fig. 5d). However, unlike WWEs, EWEs occur both west and east of the WPEE, from 140°W to 140°E (Fig. 5e). The WEI distribution of these EWEs is more normal than that of WWEs, being less skewed towards extreme values (Fig. 5f).

In this section, we have defined an index (WEI or Wind Event Index) that can be used as a proxy for the strength of the ocean response to the wind event. We showed that WWEs predominantly occur in the western Pacific and more frequently in boreal winter with a spatio-temporal structure that displays both MJO and CRW characteristics. EWEs show distinctive features from those of WWEs: they tend to occur further east, in the vicinity of the dateline, and extremely strong EWEs that could lead to significant change in SST are less frequent than extreme WWEs.

4 Relationship between intraseasonal atmospheric waves and wind events

In this section, we investigate the relationship between wind events and intraseasonal atmospheric waves, with a focus on the MJO and CRW as we did not find any wind

events modulation by convectively coupled Kelvin waves (not shown). As we will show below, there is an unambiguous modulation of wind events by the MJO and CRW, which is quite symmetric between EWEs and WWEs.

4.1 Links between MJO/CRW and wind events occurrence

Figure 6a, c shows the composite life cycle of all MJO and CRW convective phases, centred on the day and longitude where the maximum MJO or CRW-related wind stress anomaly is found. WWEs are overlaid on this composite picture. The distinctive features of the MJO and CRW can be recognised on these composites: small zonal wavenumbers and $\sim 5 \text{ m s}^{-1}$ eastward phase speed for the MJO; smaller zonal scale ($\sim 60^\circ$) and $\sim 5 \text{ m s}^{-1}$ westward phase propagation for CRW. WWEs tend to cluster along the convective phases of both MJO and CRW, with a tendency for the strongest WWEs to occur near the center of the convective phase.

Figure 6b, d provides a more quantitative assessment of the relationship between WWE and individual MJO and CRW phases. It shows the percentage of MJO/CRW

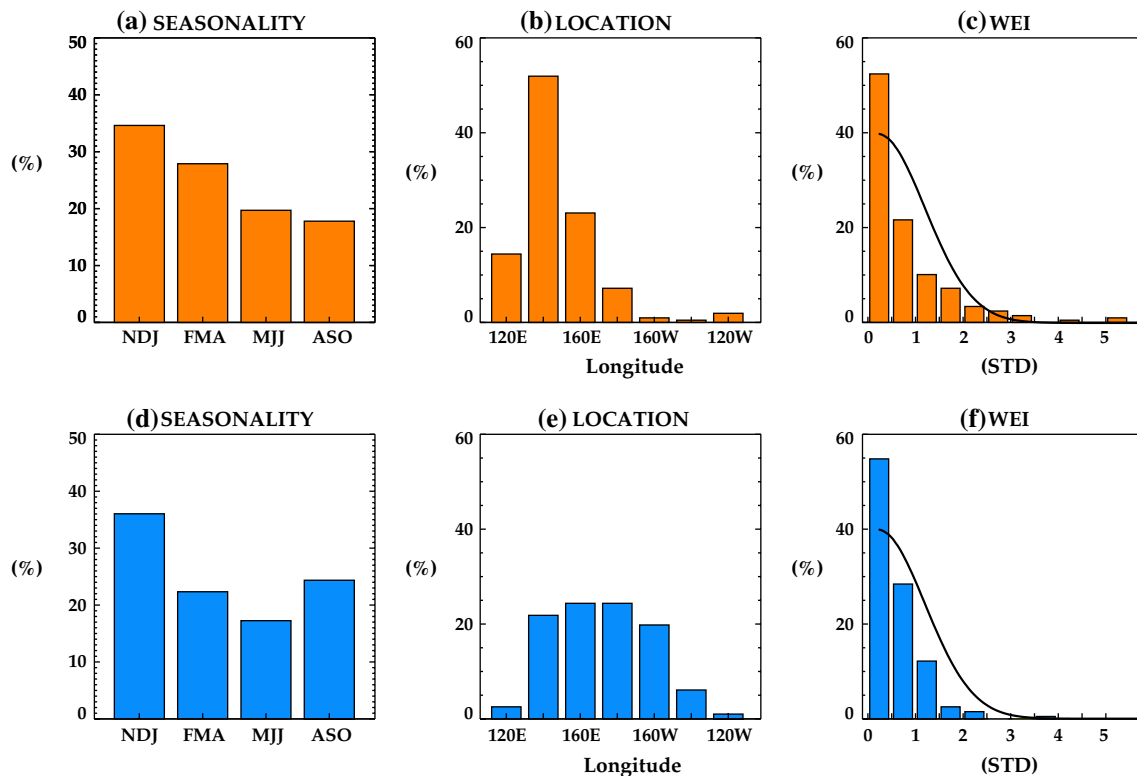


Fig. 5 WWEs (orange, a–c) and EWEs (blue, d–f) (a, d) seasonal (b, e) longitude and (c–f) Wind Event Index distributions. The black line on c and f corresponds to a normal distribution

convective and suppressed phases that contain at least one WWE and the percentage of WWEs embedded in MJO/CRW convective or suppressed phases. In order to assess the significance of this relation, we compare these percentages with the distribution obtained by randomly resampling wind events dates 10,000 times (a new occurrence year is randomly generated, and the occurrence day within the year is randomly shifted by ± 45 days). This strategy of random resampling allows preserving the WWEs seasonality, while randomly redistributing WWEs dates with respect to MJO and CRW phases. The 0.95 and the 0.05 percentile of the distribution obtained from the random sets of WWEs are represented as whiskers on Fig. 6b, d. The strategy above allows comparing the actual percentage of co-occurrence of, e.g., WWEs with the MJO with the range of percentages that would result from a completely random distribution of WWEs in time (but that still preserve the observed wind event seasonality). If, e.g., the actual co-occurrence of WWEs with the MJO exceeds the 0.95 percentile obtained by random resampling, this indicates that the association between WWEs and the MJO is significant at the 95 % confidence level.

Figure 6b shows that 60 % of the convective MJO phases are associated with WWEs and less than 2 % with suppressed phases. Reciprocally, 57 % of the WWEs are

embedded within a convective MJO phases and 1 % with suppressed phases (see also Table 2). Due to the large amount of convective CRW phases (~360), less than 38 % of convective CRW contain at least one WWE (Fig. 6d). Like the MJO case, a large part of the WWEs (70 %) are embedded in convective CRW phases and very few (<1 %) in suppressed ones.

In both cases, convective phases of MJO and CRW are not systematically associated with WWEs but much more from what would be expected with a random distribution, i.e. about 4 times more frequently. In addition, most of the WWEs occur within convective MJO and CRW phases, 3.5 times and 5 times more than would be expected from a random distribution, showing the high level of significance of these results. Conversely, almost no WWEs (less than 1 %) occur when the MJO and/or CRW phase is not favourable. Overall, convective MJO/CRW phases encompass most of the WWEs while suppressed phases encompass almost none.

The diagnostics previously used for WWEs are now applied to describe the modulation of EWEs by the MJO and CRW as shown on Fig. 7. We only briefly summarize the results, due to the rather symmetrical nature of the relation between EWEs and CRW/MJO to that of WWEs. EWEs tend to cluster along the suppressed phases of both

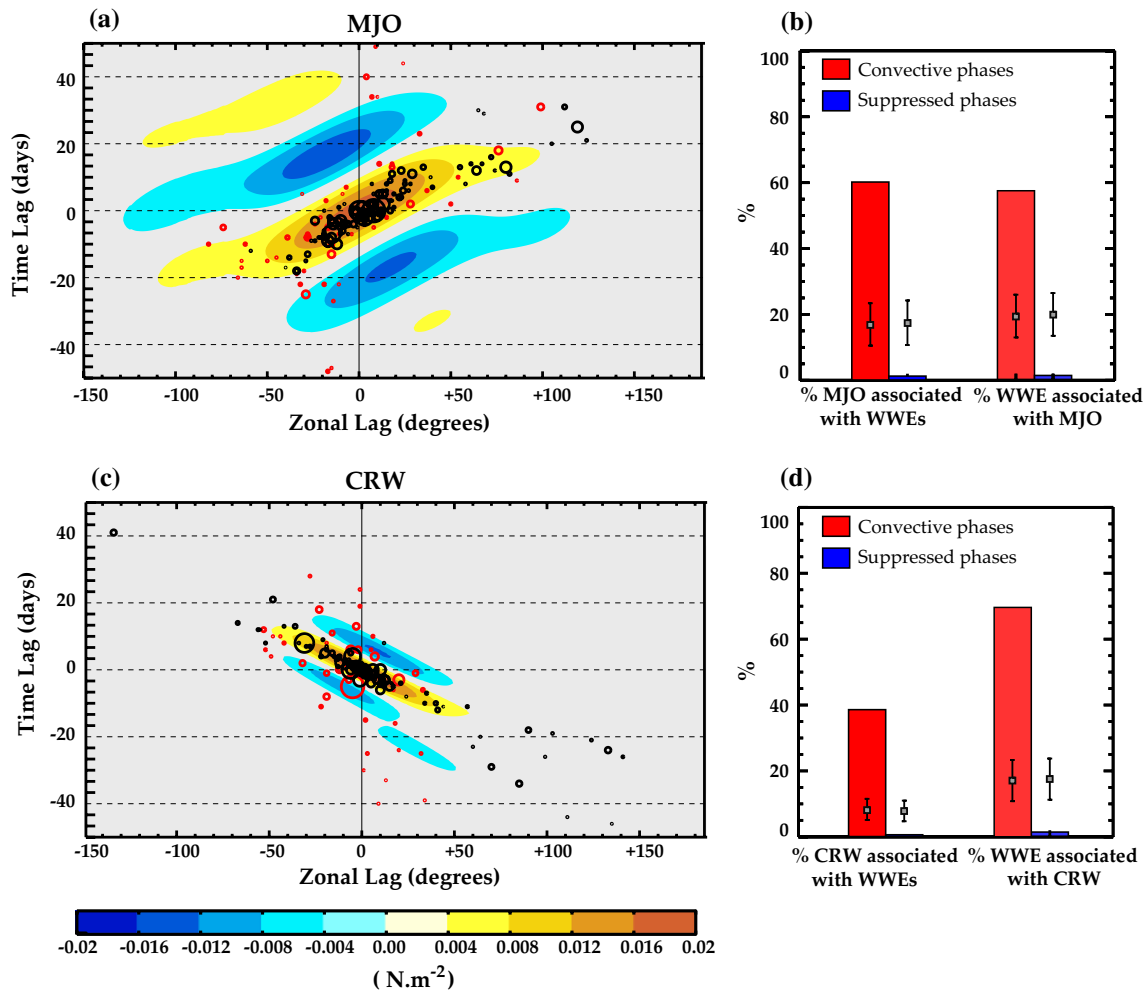


Fig. 6 (Left) Composite life-cycle of zonal wind stress anomalies associated with convective **a** MJO and **c** CRW events centred on the maximum zonal wind stress anomaly of the phase. WWEs occurrences are indicated as circles in the frame of the MJO/CRW, the size being proportional to the WEI. *Black circles* indicate WWEs that are embedded into a convective, while *red circles* indicate events that do not occur a convective phase. The inconsistencies between the *circle positions* and *colour shading* on the figure arise from the fact that the shading displays the MJO/CRW mean composite cycle, while

the *circles* refer to the wind event location relative to the instantaneous distribution of the Wheeler and Kiladis MJO and CRW indices. (Right) Percentage of convective (red bar) and suppressed (blue bar) phases containing at least one WWEs and percentage of WWEs that are embedded within convective (red bar) and suppressed (blue bar) phases for **b** MJO and **d** CRW events. The *square* indicates the percentage expected from a random distribution of the wind events in time, using a Monte-Carlo method (the *whiskers* indicate the 5 and 95 % confidence interval around that number)

MJO and CRW (Fig. 7a, c) and Fig. 7b, d indicate a strong tendency of EWEs to occur during suppressed phases of the MJO and CRW (56 and 53 % respectively, cf Table 2, about three times more than if EWEs distribution was random) and a significant tendency of MJO (51 %) and CRW (26 %) suppressed phase to induce an EWE (also above three times more that would be expected from a random occurrence of EWEs). Consistently with the weaker Rossby wave signal associated with the EWEs composite as compared to the WWEs composite (Fig. 4), the relationship between EWEs and CRW is however weaker than that of WWEs, although still highly significant.

Some WWEs occur during the co-occurrence of MJO and CRW convective phases, as for example the March 1997 WWE (Fig. 1c, d). We now investigate the combined MJO/CRW relation with WWEs occurrence. Figure 8a shows a scatterplot of the values of MJO against CRW indices at each wind event location, the size of the circle being proportional to the WEI. WWEs (shown in red/yellow/orange colours) tend to occur in the top right quadrant, corresponding to the co-occurrence of convective MJO and CRW phases (i.e. MJO and CRW normalized indices greater than 1). This relationship is further quantified on Fig. 8b, and in Table 2 that provides an exhaustive

Table 2 Percentage of EWEs (blue) and WWEs (red) occurring during each MJO/CRW phases

% of WWE (% random) % of EWE (%random)		MJO					Total: 70% (14%) 2% (14%)
		ACTIVE (= Convective + Suppressed + Transition)			NEUTRAL		
		Convective	Suppressed	Transition			
CRW	ACTIVE (= Convective + Suppressed + Transition)	Convective	41% (3%) 0% (3%)	1% (2%) 2% (2%)	4% (2%) 0% (2%)	24% (7%) 0% (7%)	Total: 1% (15%) 53% (15%)
		Suppressed	1% (3%) 3% (3%)	0% (3%) 26% (3%)	0% (2%) 2% (2%)	0% (7%) 22% (7%)	
		Transition	2% (2%) 0% (1%)	0% (1%) 1% (2%)	0% (1%) 0% (1%)	0% (4%) 0% (5%)	
NEUTRAL		13% (8%) 0% (7%)	0% (9%) 27% (9%)	0% (6%) 0% (6%)	14% (40%) 17% (41%)		
Total:		57% (16%) 3% (14%)	1% (15%) 56% (16%)				

The sketch on Fig. 2 provides an illustration of the terminology used in this table: briefly, statistics are given for neutral and active periods (active periods comprise convective, suppressed and transition phases in between). Numbers within brackets indicate the percentages that would be expected from a random distribution of wind events (see text for detail). Actual wind event distributions that are significantly larger or smaller to those expected from a random distribution are shown in bold

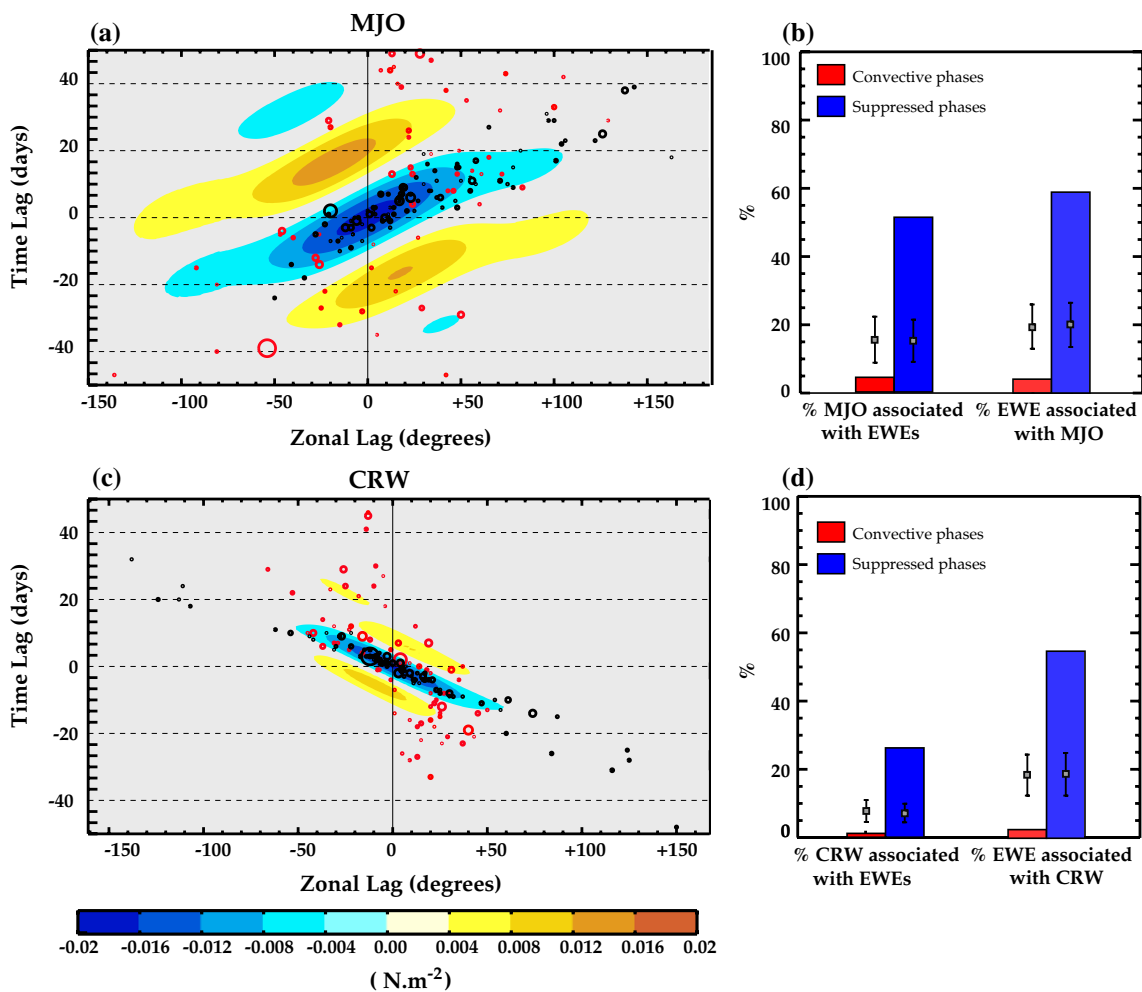


Fig. 7 Same as Fig. 6 but for EWEs

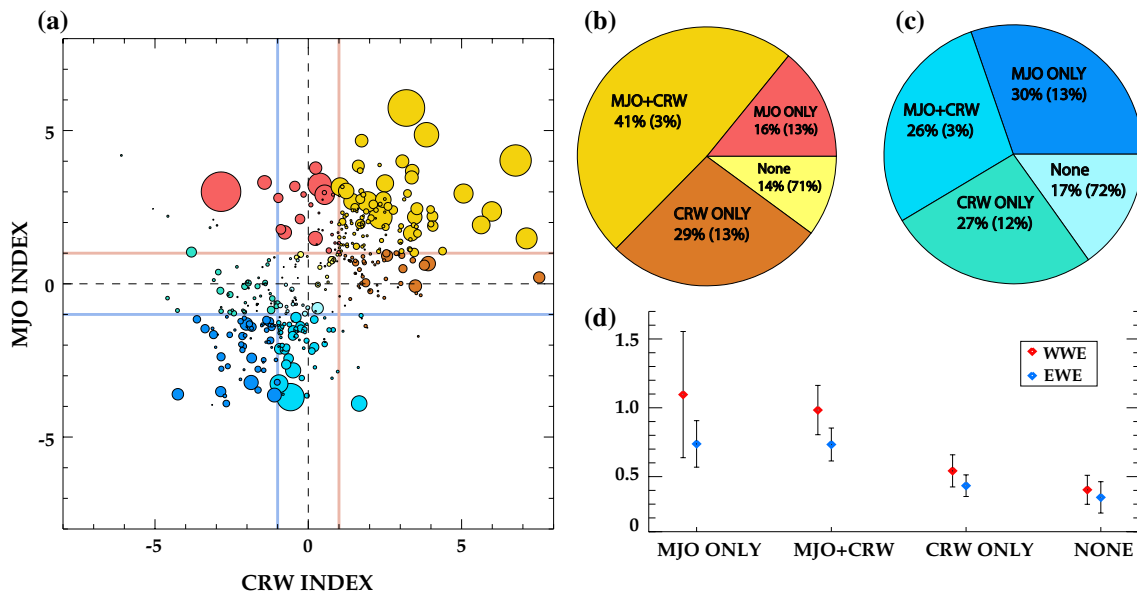


Fig. 8 a Scatter diagram of MJO against CRW indices associated with each WWE (red–yellow tones) and EWE (blue tones). The size of the dots is proportional to the Wind Event Index (WEI). Red (blue) thin lines represent the threshold for active (suppressed) MJO phases (horizontal lines) and CRW phases (vertical lines). b Percentage of WWEs embedded in MJO only, CRW only, combined MJO and CRW convective phases. c Percentage of EWEs embedded in MJO

contingency table of the percentage of wind events occurring in each MJO/CRW phases. 41 % of WWEs occur during a combined MJO and CRW convective phase while only 3 % would be expected from a random distribution of WWEs (Fig. 8b; Table 2). Similarly, 86 % (i.e. 41 % + 16 % + 29 %) of the WWEs occur during a MJO and/or CRW convective phase, when only 29 % would be expected from a random distribution.

In addition to the effect of the MJO/CRW on WWEs occurrence probability, Fig. 8a suggests an influence of the MJO/CRW activity on the strength of the WWEs as measured by the WEI, with a tendency for larger WEIs (larger circles) in the upper right quadrant. Figure 8d further confirms this visual impression: the WEI of WWEs associated with convective MJO phases is significantly larger than those associated with other atmospheric states at the 95 % confidence level. This is due to the fact that WWEs embedded in MJO tend to have a longer fetch and a longer duration, hence increasing the WEI. This is not the case for WWEs associated with the smaller scale CRW convective phases alone, which are not significantly stronger than other cases (Fig. 8d).

Similarly to WWEs, 26 % of the EWEs occur during concurrent suppressed MJO and CRW phases (Fig. 8a, c; Table 2). This is however weaker than the occurrence probability of WWEs during combined convective MJO and

only, CRW only, MJO and CRW suppressed phases. In b, c, numbers in brackets indicate the percentages that would be expected from a random distribution of wind events (see text for details). d Composite value of WWEs and EWEs WEI for wind events embedded within a MJO only, CRW only, MJO and CRW convective and suppressed phase respectively, with whiskers corresponding to the 95 % confidence interval

CRW phases (41 %) but still highly significant, i.e. seven times more than what would be expected from a random wind event distribution. Only 17 % of EWEs are not associated with either suppressed MJO or CRW phases, more than four times less than expected from a random distribution. Finally, mirroring WWEs results, EWEs embedded within a suppressed MJO phase have a significantly larger WEI than other EWEs (Fig. 8d).

In this subsection, we have shown that the rate of convective MJO and CRW phases with embedded WWEs and of WWEs within convective MJO and CRW phases are both much higher than what would be expected from a random distribution of wind events (Fig. 8b, c; Table 2). In particular, almost half of the WWEs occur during concomitant MJO and CRW convective phases, i.e. fifteen times more than would result from a random distribution. On the other hand, only MJO events appear to statistically influence the WWE strength as measured by the WEI, with significantly higher WEI associated with convective phases of the MJO than in other large-scale atmospheric situations. This analysis also shows that EWEs tend to behave symmetrically to their WWEs counterpart with regards to their relationship with MJO/CRW activity. However, our analysis reveals that EWEs have a weaker tendency to occur during CRW suppressed phase than the WWEs during CRW convective phase.

4.2 Sensitivity of the results

As mentioned in the Introduction, results from Seiki and Takayabu (2007a) and Chiodi et al. (2014) differ regarding the link between the MJO and wind events. Seiki and Takayabu (2007a) argued that 90 % of their WWEs were associated with MJO convective events over the equatorial Pacific. Chiodi et al. (2014) agree, but also concluded that WWE occurrence probability is unchanged irrespective of whether the MJO is “active” (the envelope containing both convective or suppressed phases, cf Fig. 2) or not. It is hence very important to assess the robustness of the wind events-MJO/CRW relationship with respect to the methodology. We will therefore evaluate in the following the sensitivity of our results to the atmospheric waves (MJO and CRW) detection method (Sect. 4.2.1) and to the wind event detection method (Sect. 4.2.2). For the sake of brevity, we only present results for the WWE-MJO link in this subsection, but a similar robustness is obtained when considering EWEs and/or CRW relation (not shown).

4.2.1 Sensitivity to the definition of the MJO phases

There are several other ways to characterize the Madden-Julian oscillation than the one used in the present study and derived from Wheeler and Kiladis (1999). These other options include the popular multivariate MJO index introduced by Wheeler and Hendon (2004) and used by Chiodi et al. (2014) to characterize the WWE/MJO relationship. This index consists of two time series RMM1(t) and RMM2(t) obtained through the first two principal components of the Empirical Orthogonal Functions analysis of the combined of near-equatorially-averaged 850 hPa zonal wind, 200 hPa zonal wind, and satellite-observed outgoing longwave radiation (OLR) fields (Wheeler and Hendon 2004). Together, these two time series describe both the amplitude ($RMM1^2 + RMM2^2$) and phase (position in the RMM1, RMM2 phase space) of the MJO, this phase being an indication the location of the MJO convective and suppressed phases. As our goal is to relate the occurrence of wind events to the MJO phase at the wind event position, these two time series (RMM1 and RMM2) have to be transformed into a single index, which is a function of longitude and time as for projections obtained using the Wheeler and Kiladis (1999) method. We thus use a multiple linear regression between intraseasonally-filtered equatorial wind stresses and RMM1 and RMM2 to generate $A(x)$ and $B(x)$ zonal structure functions and reconstruct the MJO induced wind stress variations as $WH_{MJO}(x,t) = A(x) * RMM1(t) + B(x) * RMM2(t)$. The resulting field is normalized by its standard deviation within 130°E to 160°W at the equator, as in Sect. 2.3.

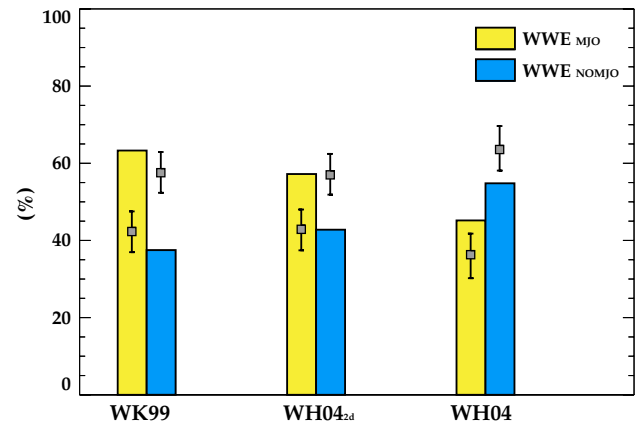
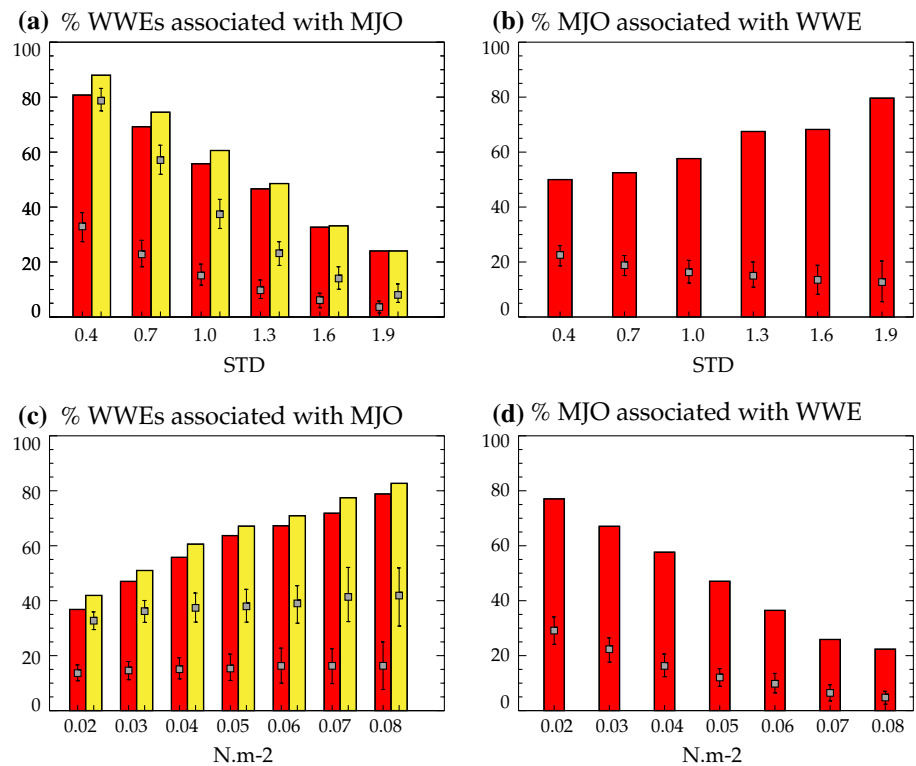


Fig. 9 Percentage of WWEs embedded in MJO active periods (WWE_{MJO} , yellow bars) and not embedded in MJO active periods (WWE_{NOMJO} , blue bars), i.e. the envelope containing both the convective and suppressed phases (see Fig. 2 for an illustration), for three MJO detection methods: Wheeler and Kiladis (1999), “spatialized” Wheeler and Hendon (2004) index (see Sect. 4.2.1 for details) and Wheeler and Hendon (2004) index. The grey squares represent the percentages expected from a random distribution of wind events in time using a Monte-Carlo method (the whiskers indicate the 5 and 95 % confidence interval around that number)

Figure 9 shows the percentage of WWEs embedded in MJO active periods (i.e. the envelope of convective and suppressed phases as illustrated on Fig. 2b) obtained using several methods for MJO detection. The first column in this figure uses the Wheeler and Kiladis (1999) method used in the present paper and indicates that 62 % of WWEs occurring during the MJO active period, while only 44 % would be expected from a random distribution of wind events. While our results agree qualitatively with Seiki and Takayabu (2007a), they thus disagree with those of Chiodi et al. (2014). While Seiki and Takayabu (2007a) used band-pass filtered (10–100 days) potential velocity at 200 mbar in the vicinity of WWEs to characterize the MJO state, Chiodi et al. (2014) defined the MJO using the amplitude of the Wheeler and Hendon (2004) index. The sensitivity of the MJO/WWE relationship to the MJO definition is further illustrated on Fig. 9, which also shows the percentage of WWEs embedded in MJO active periods using the Wheeler and Hendon (2004) index (RMM) and a spatialized version of this index. To define the MJO using RMM, we did as in Chiodi et al. (2014) where the MJO is considered active when the RMM index amplitude is >1 for at least 20 consecutive days and inactive when not. The larger rate of WWEs occurrence within MJO active periods than if WWEs were occurring randomly is verified with the three indices, although it is hardly significant when using the Wheeler and Hendon (2004) index. The differences between our results and Chiodi et al. (2014) are hence probably due to the use of the Wheeler and Hendon

Fig. 10 (Left) Percentage of WWEs embedded in a convective (red bars) and an active period (yellow bars) MJO phase and (right) percentage of convective MJO phases with at least a WWE as a function of increasing wind stress criterion for (upper) WWEs selection and (lower) MJO phases selection. The grey bars indicate the value that would be expected from a random distribution of wind events (see text for details)



(2004) index in their study. Using a one-dimensional MJO index such as RMM led to a far less significant relationship between WWEs and the MJO compared to indices with a much larger number of degrees of freedom such as Wheeler and Kiladis (1999). While indices such as Wheeler and Hendon (2004) capture the MJO activity at global scale, they indeed do not necessarily accurately depict more local MJO signals over the Pacific warm pool.

Our results may not only be sensitive to the MJO detection method but also to the threshold used to characterize the MJO state (suppressed, neutral or convective). Figure 10a shows the percentage of WWEs embedded in MJO convective and active periods, when the MJO convective phase threshold varies from 0.4 to 1.9 standard deviations using the Wheeler and Kiladis (1999) MJO detection method. When this threshold increases, the number of MJO convective and active periods decreases, and the percentage of WWEs associated with a convective MJO phase thus also decreases. However, this percentage always remains above what would be expected from a random distribution of WWEs. It is also interesting to note that while the percentage of WWEs embedded in a MJO active period (yellow bars on Fig. 10a) is close, although still significantly higher, to what could be expected from a random distribution for low MJO thresholds (std lower than 1), this percentage is more than twice larger than for a random distribution using more stringent MJO thresholds (std larger than 1). This illustrates that the tendency of active MJO events

to favour the occurrence of WWEs is more pronounced for MJO events of large amplitude. Figure 10b depicts the percentage of MJO convective phases that contain at least a WWE, when the MJO convective phase criterion varies from 0.4 to 1.9 standard deviations. This percentage increases from 50 % (for weak MJO, 0.4 std) to more than 80 % (for strong MJO, 1.9 std), illustrating again that the strongest MJO are very likely to contain at least one WWE. In addition, the percentage of MJO convective phases that contain at least one WWE is always significantly larger (up to four times) than the one expected from a wind event random distribution. Similar results are also obtained when using the Wheeler and Hendon (2004) MJO detection method (not shown). Overall, our results about the relationship between wind events and the MJO/CRW are hence robust, irrespective of detection method and the choice of MJO and CRW detection criteria.

4.2.2 Sensitivity to wind events criteria

Another source of sensitivity of our results may arise from the criterion used for the wind events detection method, which varies significantly from one study to another (Table 1). In this subsection, we therefore assess the sensitivity of our results with respect to this criterion. Figure 10c shows the percentage of WWEs associated with MJO convective and active periods, for a WWE detection criterion ranging from 0.02 to 0.08 N m⁻². First, WWEs occur more

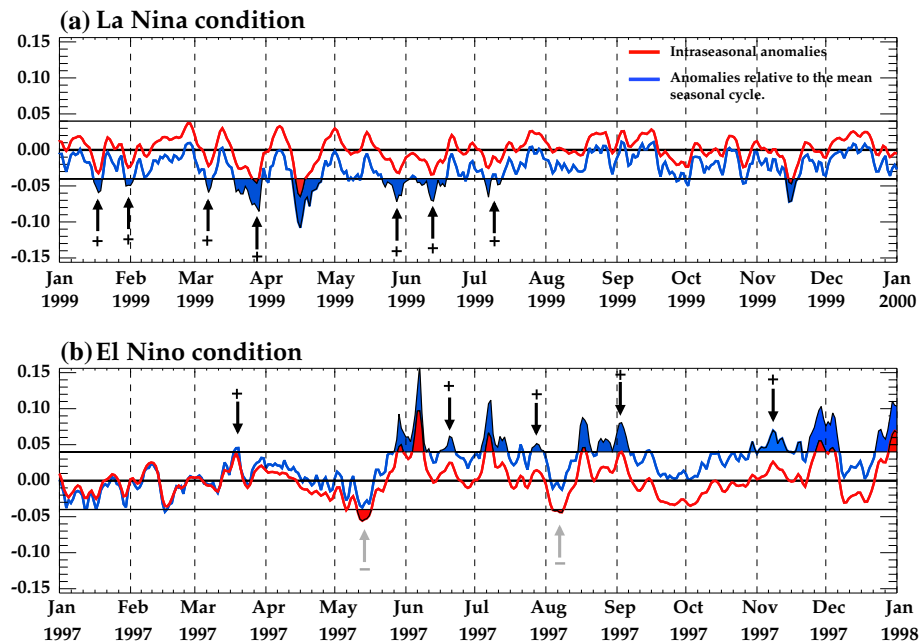


Fig. 11 Time series of zonal wind stress intraseasonal (red) and interannual anomalies (blue) in the $[5^{\circ}\text{N}\text{--}5^{\circ}\text{S}; 155^{\circ}\text{E}\text{--}180^{\circ}]$ box during **a** the 1998–1999 La Niña and **b** 1997–1998 El Niño. The horizontal black lines indicate the -0.04 and 0.04 N m^{-2} thresholds used to detect EWEs and WWEs. Areas filled in blue indicate the detected wind events using anomalies with respect to the seasonal cycle and

areas filled in red with intraseasonal anomalies. Wind events detected only with the method based on anomalies with respect to the seasonal cycle are labelled by an arrow with a plus while wind events detected only detected when using a detection method based on intraseasonal anomalies are labelled by an arrow with a minus

frequently during convective and active MJO phases than what would be expected from a random WWE distribution whatever the WWE criterion selected. Second, the percentage of WWEs associated with MJO convective and active periods increases when the WWE magnitude threshold increases, a clear indication that stronger WWEs are more systematically associated with MJO convective and active periods than weaker ones, as suggested by Seiki and Takayabu (2007a). Figure 10d further shows percentage of MJO convective phases containing at least a WWE, for a WWE detection criterion ranging from 0.02 to 0.08 N m^{-2} . This panel illustrates that convective MJO phases are more associated with WWEs than would be expected from a random WWE distribution for various choices of the detection threshold. Overall, our main results about the relationship between wind events and the MJO/CRW are hence robust, irrespective of the choice of wind event detection criterion.

5 Relationship between background interannual variations and wind events

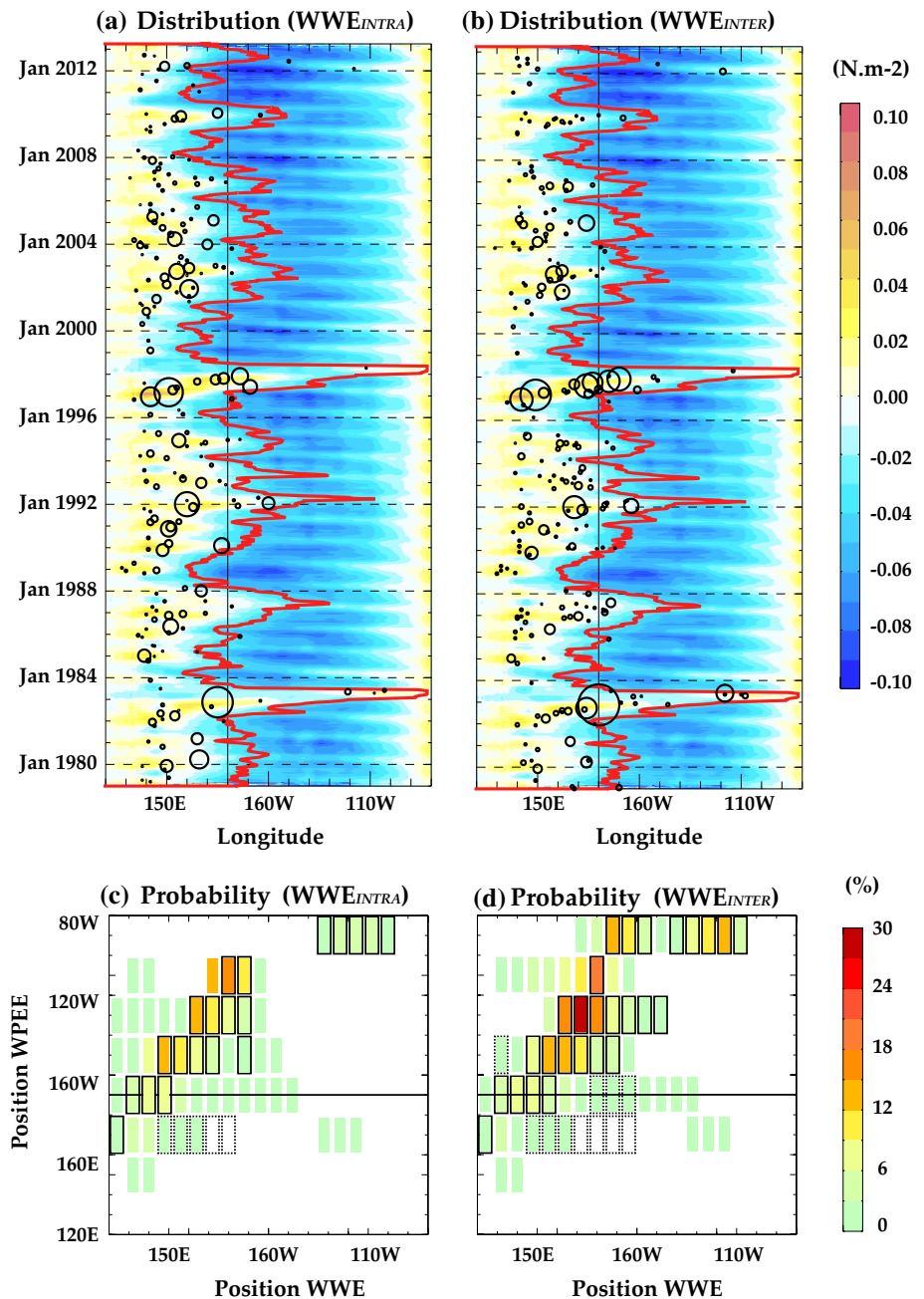
Previous studies generally agree on the tendency of WWEs to be more likely prior to and during most El Niño events (Harrison and Vecchi 1997; Eisenman et al. 2005; Seiki and Takayabu 2007a; Chiodi et al. 2014), i.e. when the warm

pool is anomalously extended eastward. Chiodi and Harrison (2015) suggest that EWEs also vary with ENSO state, with an increased probability of EWEs occurrence during La Niña conditions. In the aforementioned studies, WWEs were detected from zonal wind or wind stress anomalies with respect to the mean seasonal cycle, while we detect wind events based on intraseasonally-filtered wind stress (see Table 1). In the following section, we will assess the implication of the way the wind events are defined on their relationship with background interannual SST variations.

5.1 Robustness of wind event interannual modulation

The way wind events are defined can indeed strongly bias the ENSO-wind event relationship, because the zonal winds display strong ENSO-related interannual variability (i.e. easterly anomalies during La Niña and westerly anomalies during El Niño) and wind events identification schemes based on interannual anomalies by construction detect more WWEs during El Niño years. This methodological caveat is illustrated on Fig. 11 that compares wind events detected either with intraseasonal anomalies or anomalies relative to the seasonal cycle during the 1998–1999 La Niña and 1997–1998 El Niño. During La Niña conditions, the negative interannual anomalies favour the detection of EWEs when wind events are detected based on interannual

Fig. 12 (Top) Average 2°N–2°S time-longitude section of 90-day low-pass filtered zonal wind stress over 1979–2012, with circles indicating WWEs detected using **a** intraseasonal zonal wind stress anomalies (referred as WWE_{INTRA}) and **b** anomalies relative to a mean seasonal cycle (referred as WWE_{INTER} ; see beginning of Sect. 5.1 for more details). The size of the circles is proportional to the Wind Event Index the red line indicate the eastern edge of the warm pool. (Bottom) Zonal distribution of the WWE occurrence probability (%), as a function of the position of the eastern edge of the warm pool for **c** WWE_{INTRA} and **d** WWE_{INTER} . The WWEs occurrence probability (%) is computed as the ratio of the total duration of WWEs for a given longitude and position of the WPEE to the total number of days for which the WPEE is at this longitude. Black solid (dashed) boxes represent bins where the wind event occurrence probability is significantly higher (lower) than what would be expected with a random distribution at the 95% confidence level. The black line indicates the mean position of the warm pool eastern edge



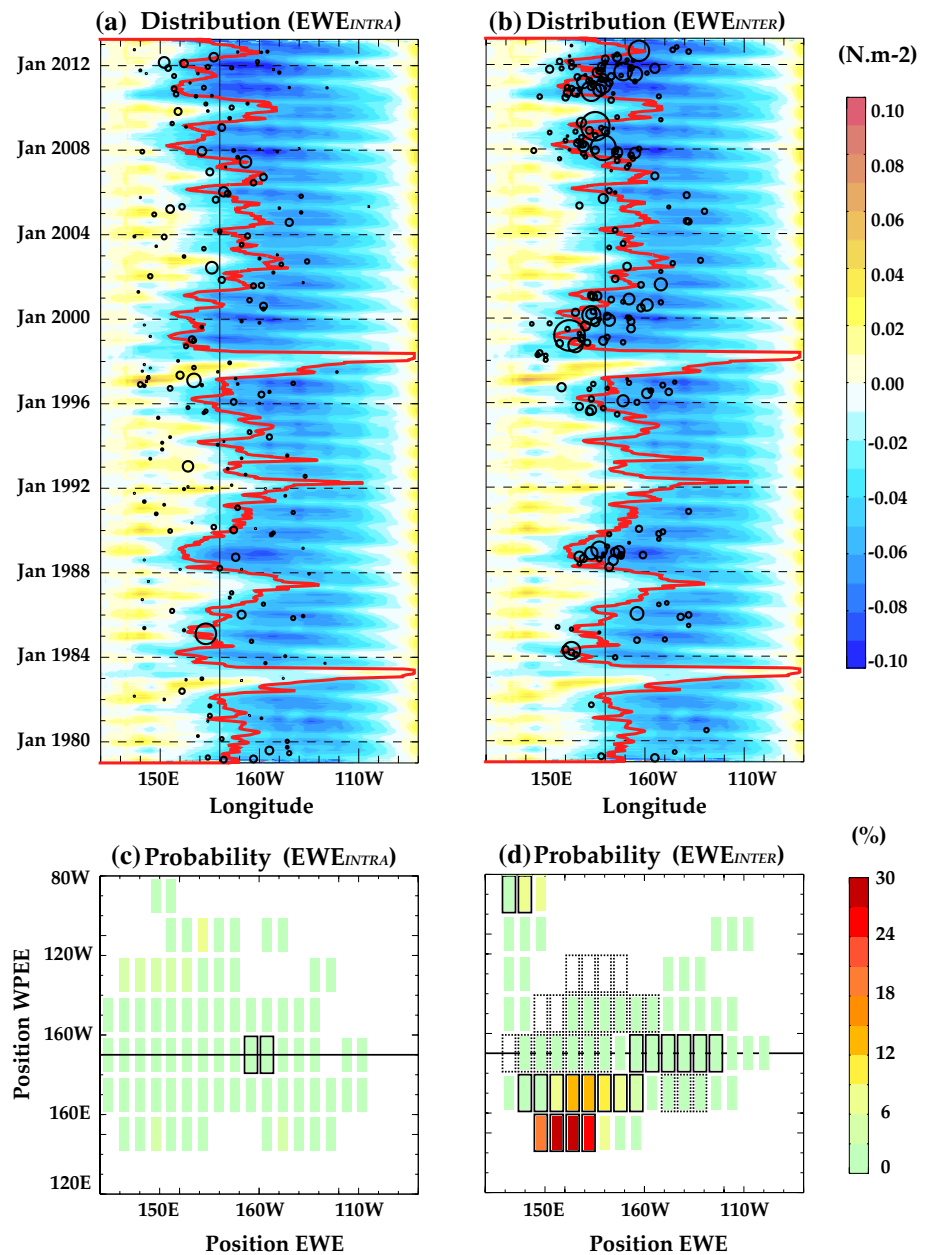
anomalies using the same thresholds. Symmetrically, more WWEs are detected during El Niños when using a detection method based on anomalies with respect to the mean seasonal cycle.

Comparing Fig. 12a, b allows illustrating the differences in the WWEs detected using intraseasonal anomalies as in the present study (hereafter “ WWE_{INTRA} ”) or from interannual anomalies as in most previous studies (hereafter “ WWE_{INTER} ”) detection). Both WWEs detection methods yield WWEs that mostly occur in the western pacific, west of the WPEE and follow WPEE interannual displacement. These panels also suggest that strongest WWEs in terms

of WEI occur when the WPEE is shifted to the east. This comparison therefore suggests that the WWEs relationship with background SST interannual variations is not qualitatively affected by the WWEs detection method.

A more quantitative assessment of the sensitivity relationship to the WWEs detection method is further provided on Fig. 12c, d, which shows the zonal distribution of WWEs occurrence probability as a function of the WPEE position for the WWE_{INTRA} (Fig. 12c) and WWE_{INTER} (Fig. 12d) detection methods. The WWEs occurrence probability is computed as the ratio of the total duration of WWEs for a given longitude and position of the WPEE to the total

Fig. 13 Same as Fig. 11 but for EWEs

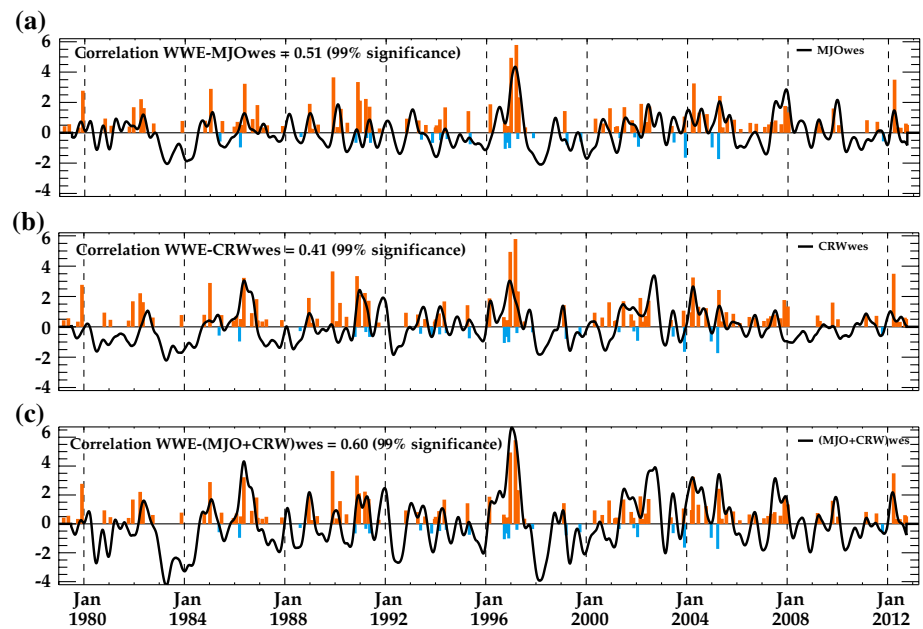


number of days for which the WPEE is at this longitude. The WWE_{INTRA} method yields WWE that are on average 3 times more likely to occur in the central Pacific when the warm pool extends eastward of the date line, and less likely to occur when the warm pool is restricted to the far western Pacific (Fig. 12c). This is consistent with previous studies (Lengaigne et al. 2003; Eisenman et al. 2005; Vecchi et al. 2006; Gebbie et al. 2007) which argued that the eastward expansion of the warm pool eastward increases the areal extent of warm water over which subsequent WPEEs can force the ocean, and result in further interannual WPEE eastward expansion. Comparing Fig. 12c with d however clearly illustrates that detecting WPEEs from anomalies

with respect to the mean seasonal cycle artificially enhance the modulation of WPEEs by ENSO. WWE_{INTER} are indeed four times more likely to occur when the warm pool is shifted east the date line (Fig. 12d), compared to three times more likely for WWE_{INTRA} (Fig. 12c). Similarly, WWE_{INTER} are three times less likely when the warm pool is displaced in the far western Pacific as compared to two times less likely for WWE_{INTRA} . Despite this sensitivity, these results however indicate that the WPEEs occurrence modulation by the warm pool position is a robust feature, whatever detection method is used.

An analysis similar to Fig. 12 is provided on Fig. 13, but for EWEs. Comparing Fig. 13a, b reveals that, in contrast

Fig. 14 Time series of **a** MJO, **b** CRW and **c** MJO + CRW interannual activity indices (see text for details) in the western Pacific (120°E – 155°E), with the WEI value for each WWE (orange) and EWE (blue) in the same box overlaid. WEI values are correlated at 0.51 with the MJO, 0.41 with the CRW and 0.60 with the MJO + CRW interannual activity index for WWEs, while this correlation is insignificant for EWEs



to WWEs, the method used to detect EWEs strongly alter the ENSO–EWEs relationship: while $\text{EWE}_{\text{INTER}}$ tend to cluster just east of the WPEE during La Niña events and nearly vanish during El Niño events (Fig. 13b), in line with Chiodi and Harrison (2015) results, $\text{EWE}_{\text{INTRA}}$ do not exhibit any clear modulation by interannual SST variability (Fig. 13a). Comparing Fig. 13c with 13d further confirms that the EWEs relationship with interannual background SST is very sensitive to the EWEs detection method. The significant link between interannual SST variability and $\text{EWE}_{\text{INTER}}$ evident on Fig. 13d disappears completely when considering $\text{EWE}_{\text{INTRA}}$ (Fig. 13c). The implications of this asymmetry between EWEs and WWEs occurrence in terms of their relation with ENSO variability will be further discussed in Sect. 6.3.

5.2 Modulation of wind events by MJO/CRW interannual variations

Seiki and Takayabu (2007a) did not find any relationship between the MJO and WWEs occurrence at interannual timescale. In this subsection, we re-examine their result and explore if interannual MJO and/or CRW variations contribute to the wind events modulation at interannual timescales. Following a similar strategy to that described in Hendon et al. (2007), we define an interannual MJO activity index ($\text{MJO}_{\text{inter}}$) as the standard deviation of the MJO index defined in Sect. 2 over a 90 day sliding window, averaged over the western Pacific (120°E – 155°). The mean seasonal cycle of that index is then removed to highlight interannual

variations of the MJO activity. A similar index is computed for CRW activity ($\text{CRW}_{\text{inter}}$). Figure 14a,b shows these two indices, along with the WEI of each EWE and WWE in the 120° – 155°E region.

As suggested by Figs. 1c, d, 14a, b confirms that the MJO and CRW activity was anomalously strong during the onset of the 1997 El Niño event and associated with intense WWEs activity. But this relationship does not hold for every El Niño event: for instance, the strong WWEs activity preceding the 1992 El Niño is barely associated with any anomalous MJO activity. Over the entire period, we however find a 0.51 correlation between the WWEs WEI and the synchronous MJO activity index at interannual timescales (Fig. 14a, b). The relationship between wind events and CRW interannual variability is weaker, with a 0.41 correlation. The sum of the MJO and CRW indices further increases this correlation to 0.6 (Fig. 14c). These correlations are all statistically significant at the 95 % significance level (one-tailed t test with the numbers of effective degrees of freedom estimated as in Livezey and Chen 1983) and remain significant when the strong 1997–1998 El Niño period is not taken into account. This indicates that wind events tend to be stronger, have a larger fetch or last longer (three factors that contribute to the WEI) during periods of anomalously high interannual MJO and/or CRW activity. Part of the of the WWEs intensity interannual variability can thus be interpreted as resulting from interannual variations of the MJO and CRW activity (either internal or ENSO-driven). This relation however does not hold for WWEs located in the central/eastern pacific, nor for EWEs (not shown).

6 Summary and discussion

Several studies have proposed that WWEs, and more recently EWEs, influence the ENSO cycle. The question whether these short-lived episodic wind events occur randomly or are to some extent modulated by large-scale modes, such as ENSO at interannual timescales or the Madden–Julian oscillation at intraseasonal timescales, is important, because such a control could potentially increase wind events predictability and therefore ultimately improve ENSO prediction. Several papers already addressed the relationship between WWEs and large-scale variability, sometimes leading to contradictory results. The present paper aims at revisiting this question.

6.1 Main wind events characteristics

In the present study, we use a WWEs/EWEs detection method applied to intraseasonal wind stress anomalies from TropFlux data from 1979 to 2012. Identifying wind events based on wind stress rather than wind speed was implemented in order to focus on events with a potentially strong oceanic impact. To this end, we also focus on wind events that exhibit rather large-amplitude, long duration and large zonal fetch, using the rather conservative thresholds of 0.04 N m^{-2} , 5 days and 10° . In agreement with previous studies, we show that WWEs occur in the western Pacific, usually west of the eastern edge of the warm pool, and more frequently in boreal winter than in boreal summer. While EWEs are to a large extent the easterly counterpart of WWEs, they also show distinctive features. Compared to WWEs, they tend to occur further east, i.e. in the vicinity of the dateline. Exceptionally strong EWEs are also less frequent than exceptionally strong WWEs.

6.2 Relationship with atmospheric waves

While a large body of literature suggests that MJO events modulate the intensity and frequency of WWEs over the western Pacific (e.g. Lau et al. 1989; Yu and Rienecker 1998; McPhaden 1999), the only two studies that assessed quantitatively the WWEs/MJO relationship led to contradictory results: while Chiodi et al. (2014) argued that the WWEs probability of occurrence does not change if the MJO is active or not, Seiki and Takayabu (2007a, b) concluded that large-amplitude active MJO periods increase the WWEs probability of occurrence. Our results unambiguously demonstrate that the WWEs probability occurrence significantly increases during the convective MJO events, with 57 % of WWEs embedded in a MJO convective phase (Table 2). In addition, our results indicate that 62 % of WWEs occurs during the MJO active period (i.e. the envelope containing both convective or suppressed

phases), while only 44 % would be expected from a random distribution of wind events. Our results therefore support Seiki and Takayabu (2007a). We further suggest that the disagreement between Seiki and Takayabu (2007a) and Chiodi et al. (2014) can largely be explained by the different methodologies used to define MJO events in these two studies: while Seiki and Takayabu (2007a) used an index in the vicinity of WWEs to characterize the MJO state, the Wheeler and Hendon (2004) index used by Chiodi et al. (2014) is meant to capture the MJO activity at global scale and may not accurately depict the more local MJO signals over the western Pacific.

In addition to MJO activity, previous studies also argued that WWEs were frequently associated with cyclone pairs (Keen 1982; Harrison and Giese 1991; Yu and Rienecker 1998). Seiki and Takayabu (2007a) further suggested that these cyclone pairs are the surface signatures of enhanced atmospheric Rossby waves activity during WWEs occurrence, but did not quantify this relationship. Our results reveal that the WWEs probability occurrence significantly increases with CRW activity, with 70 % of WWEs embedded during a CRW convective phase (Table 2). In addition, we show that about half of WWEs also occur during a combined CRW and MJO convective phase, i.e. about fifteen times more than what would be expected from a random distribution of WWEs (3 %, Table 2).

Results from the present study also demonstrate that EWEs largely mirror WWEs in their relationship to MJO/CRW activity: EWEs occur more frequently than would be expected from a random distribution during the suppressed phase of MJO and CRW (and like for WWEs, this result also holds for active periods as a whole; not shown). The association between EWEs and large-scale atmospheric waves is however weaker than for WWEs. A weaker proportion of EWEs (53 %) for instance occurs during CRW suppressed phase, as compared with WWEs occurring during CRW convective phases (70 %, Table 2).

6.3 Relationship with ENSO

In this study, we have also assessed the robustness of the link between wind events occurrence probability and ENSO-related warm pool movements. The increased number of WWEs prior and during El Niño warm events has been noted by numerous studies (Verbickas 1998; Kerr 1999; McPhaden 2004; Eisenman et al. 2005; Seiki and Takayabu 2007a, b). Chiodi and Harrison (2015) also indicated a mirror relationship for EWEs, with an increased EWEs probability during La Niña events. In those studies, wind events were detected from anomalies with regards to the mean seasonal cycle. This method may however bias the ENSO-wind event relationship, because El Niño positive and La Niña negative zonal wind stress low frequency

anomalies will favour more WWE and EWEs detections respectively (see Fig. 11). We revisited these results using a wind event detection method based on intraseasonally filtered wind stress (i.e. that does not include the interannual component for the wind event detection). Our results show that detecting WWEs from intraseasonal anomalies still yields an increasing WWEs occurrence probability when the warm pool is displaced eastward during El Niño events, and a decreasing WWEs probability during La Niña events. We also demonstrate that WWEs tend to be stronger during periods of anomalously high interannual MJO and/or CRW activity, indicating that part of the interannual variability of the WWEs intensity can be interpreted as resulting from interannual variations of the MJO and CRW activity (either driven randomly or by the ENSO-related interannual modulations of the warm pool extension). In contrast, this relationship with ENSO completely vanishes when EWEs are detected based on intraseasonal wind stress anomalies. Our results hence underline the robustness of the ENSO–WWEs relationship but question ENSO–EWEs relations.

Several studies have shown that WWE-driven eastward displacement of the WPEE enhance the probability of further WWEs (Perigaud and Cassou 2000; Lengaigne et al. 2003, 2004b; Vecchi et al. 2006; Gebbie et al. 2007). Using state-dependent instead of additive stochastic forcing in simple (Jin et al. 2007), intermediate (Eisenman et al. 2005; Perez et al. 2005), hybrid (Gebbie et al. 2007) and general circulation models (Lopez et al. 2013) increases ENSO amplitude (Eisenman et al. 2005; Gebbie et al. 2007) and affects its predictability. The ENSO-dependent nature of the wind events stochastic forcing is thus critical to ENSO properties (e.g. Lengaigne et al. 2004a; Vecchi et al. 2006; Eisenman et al. 2005; Gebbie et al. 2007; Gebbie and Tziperman 2009a, b). An added value of the present study is to indicate that most of the state-dependency of WWEs to ENSO SST variations is mediated by the modulation of the MJO and CRWs (cf Sect. 5.2 and Fig. 14). While the present study further confirms the ENSO-dependent nature of WWEs, the EWEs state dependence suggested by Chiodi and Harrison (2015) strongly depends on the way EWEs are defined and is hence less robust than for WWEs. When considered as purely intraseasonal events, EWEs cannot be considered as a state-dependent forcing, making their impact on the coupled system probably less likely than that of WWEs. On the other hand, the increased EWEs frequency obtained on the basis of interannual anomalies detection during La Niña could also be interpreted as EWEs being the cause of La Niña trade strengthening. The absence of relationship between ENSO and EWEs defined as purely intraseasonal events however suggests that EWEs may interact less with their large-scale environment than WWEs. The WWEs energetics analysis of Seiki and Takayabu (2007b) suggest that interaction with the large-scale

environment contributed to the increase in kinetic energy close to the equator during WWEs. A similar study for EWEs may allow understanding why they interact less with the large-scale environment.

6.4 Conclusion and perspectives

We showed that westerly and easterly wind events occur significantly more frequently during the active period of the MJO and CRW. We also confirmed that WWEs occurrence is robustly modulated by the ENSO-related interannual displacements of the warm pool, while the dependence of EWEs probability occurrence on interannual variability is highly sensitive to the wind event detection method. These findings may however not result in a drastic improvement of wind events predictability. MJO events remain rather poorly predicted beyond 10 days lead time (Rashid et al. 2010) and the CRW predictability remain unknown. In addition, only stronger MJO events are almost systematically associated to wind events, while considering all events yields a wind event occurrence probability of only 40–50 %. As a result, there is only a limited potential for wind event predictability at intraseasonal timescales. The improvement of WWEs predictability resulting from their relationship with ENSO may also be limited. The recent 2014 Pacific evolution is a good illustration of this. Early 2014 was indeed characterized by an anomalously high ocean heat content and two strong WWEs that triggered an eastward displacement of the warm pool and strong downwelling Kelvin waves, in a very similar way to during the onset of the 1997 El Niño event. The similarities between these two periods prompted a number of experts to wonder if an El Niño matching the extreme 1997/98 El Niño could develop in 2014. However, the similar eastward shift of the warm pool in the first months of 1997 and 2014 did produce very different WWEs sequences. While several WWEs occurred in boreal spring and summer 1997 and contributed to the ENSO growth, no subsequent WWEs occurred from April to July in 2014, ruling out the possibility of a strong El Niño at the end of 2014 (Menkes et al. 2014). The reason behind the different atmospheric responses to a similar warm pool eastward shift is a key issue to be addressed. These results echo the modelling results of Lengaigne et al. (2004b) who suggested that a strong WWE-driven displacement of the warm pool in the early part of the year could result in very different El Niño amplitude. The stochastic part of the WWEs occurrence during El Niño onset phase may therefore be large enough to strongly affect the subsequent El Niño evolution and may therefore be an intrinsic limitation of the predictability of ENSO amplitude. Assessing the predictability of WWEs occurrence therefore deserves further investigation.

Acknowledgments We acknowledge fruitful discussions with Andy Chiodi and Ed Harrison. This work was partially funded by the Agence Nationale pour la Recherche ANR-10-Blanc-616 METRO project. We also thank the reviewers for their comments that helped clarifying this manuscript. Martin Puy is funded by a Ministère de l'Enseignement Supérieur et de la Recherche (MESR) PhD grant. Jérôme Vialard and Matthieu Lengaigne are funded by Institut de Recherche pour le Développement (IRD). Eric Guilyardi is funded by the Centre National de la Recherche Scientifique (CNRS, France) and by the National Centre for Atmospheric Science (UK).

References

- Barnston A, Tippett MK, L'Heureux ML, Li S, DeWitt DG (2012) Skill of real-time seasonal ENSO model predictions during 2002–2011: is our capability increasing? *Bull Am Meteorol Soc* 93:631–651. doi:[10.1175/BAMS-D-11-00111.1](https://doi.org/10.1175/BAMS-D-11-00111.1)
- Bergman JW, Hendon HH, Weickmann M (2001) Intraseasonal air–sea interactions at the onset of El Niño. *J Clim* 14:1702–1719. doi:[10.1175/1520-0442\(2001\)014<1702:IASIAT>2.0.CO;2](https://doi.org/10.1175/1520-0442(2001)014<1702:IASIAT>2.0.CO;2)
- Bjerknes J (1969) Atmospheric teleconnections from the equatorial Pacific. *Mon Weather Rev* 97:163–172. doi:[10.1175/1520-0493\(1969\)097<0163:ATFTEP>2.3.CO;2](https://doi.org/10.1175/1520-0493(1969)097<0163:ATFTEP>2.3.CO;2)
- Boulanger JP, Menkes C (1999) Long equatorial wave reflection in the Pacific Ocean from TOPEX/POSEIDON data during the 1992–1998 period. *Clim Dyn* 15:205–225. doi:[10.1007/s003820050277](https://doi.org/10.1007/s003820050277)
- Boulanger JP, Durand E, Duvel JP, Menkes C, Delecluse P, Imbard M, Lengaigne M, Madec G, Masson S (2001) Role of non-linear oceanic processes in the response to westerly wind events: new implications for the 1997 El Niño onset. *Geophys Res Lett* 28:1603–1606. doi:[10.1029/2000GL012364](https://doi.org/10.1029/2000GL012364)
- Boulanger JP, Menkes C, Lengaigne M (2004) Role of high- and low-frequency winds and wave reflection in the onset, growth and termination of the 1997/1998 El Niño. *Clim Dyn* 22(267):280. doi:[10.1007/s00382-003-0383-8](https://doi.org/10.1007/s00382-003-0383-8)
- Chang CP, Erickson JE, Lau KM (1979) Northeasterly cold surges and near-equatorial disturbances over the winter MONEX area during December 1974. Part I: synoptic aspects. *Mon Weather Rev* 107:812–829. doi:[10.1175/1520-0493\(1979\)107<0812:NCSANE>2.0.CO;2](https://doi.org/10.1175/1520-0493(1979)107<0812:NCSANE>2.0.CO;2)
- Chen SS, Houze RA (1997) Interannual variability of deep convection over the tropical warm pool. *J Geophys Res* 102:25783–25795. doi:[10.1029/97JD02238](https://doi.org/10.1029/97JD02238)
- Chen SS, Houze RA, Mapes BE (1996) Multiscale variability of deep convection in relation to large-scale circulation in TOGA COARE. *J Atmos Sci* 53:1380–1409. doi:[10.1175/1520-0469\(1996\)053<1380:MVODCI>2.0.CO;2](https://doi.org/10.1175/1520-0469(1996)053<1380:MVODCI>2.0.CO;2)
- Chiodi A, Harrison DE (2015) Equatorial Pacific easterly wind surges and the onset of La Niña Events. *J Clim* 28:776–792. doi:[10.1175/JCLI-D-14-00227.1](https://doi.org/10.1175/JCLI-D-14-00227.1)
- Chiodi A, Harrison DE, Vecchi GA (2014) Subseasonal atmospheric variability and El Niño waveguide warming: observed effects of the Madden–Julian oscillation and Westerly Wind Events. *J Clim* 27:3619–3642. doi:[10.1175/JCLI-D-13-00547.1](https://doi.org/10.1175/JCLI-D-13-00547.1)
- Dee DP et al (2011) The ERA-Interim reanalysis: configuration and performance of the data assimilation system. *Q J R Meteorol Soc* 137(553):597. doi:[10.1002/qj.828](https://doi.org/10.1002/qj.828)
- Delcroix T, Eldin G, McPhaden MJ, Morlière A (1993) Effects of westerly wind bursts upon the Western Equatorial Pacific ocean, February–April 1991. *J Geophys Res* 98:16379–16385. doi:[10.1029/93JC01261](https://doi.org/10.1029/93JC01261)
- Drushka K, Bellenger H, Guilyardi E, Lengaigne M, Vialard J, Madec G (2015) Processes driving intraseasonal displacements of the eastern edge of the warm pool: the contribution of westerly wind events. *Clim Dyn* 44:735–755. doi:[10.1007/s00382-014-2297-z](https://doi.org/10.1007/s00382-014-2297-z)
- Eisenman I, Yu L, Tziperman E (2005) Westerly Wind Bursts: ENSO's Tail Rather than the Dog? *J Clim* 18:5224–5238. doi:[10.1175/JCLI3588.1](https://doi.org/10.1175/JCLI3588.1)
- Eldin G, Delcroix T, Hémin C, Richards K, du Penhoat Y, Picaut J, Rual P (1994) Large-scale current and thermohaline structures along 156°E during the COARE intensive observation period. *Geophys Res Lett* 21:2681–2684. doi:[10.1029/94GL01166](https://doi.org/10.1029/94GL01166)
- Fasullo J, Webster PJ (2000) Atmospheric and surface variations during westerly wind bursts in the tropical western Pacific. *Q J R Meteorol Soc* 126:899–924. doi:[10.1002/qj.49712656407](https://doi.org/10.1002/qj.49712656407)
- Fedorov AV (2002) The response of the coupled tropical ocean–atmosphere to westerly wind bursts. *Q J R Meteorol Soc* 128:1–23. doi:[10.1002/qj.200212857901](https://doi.org/10.1002/qj.200212857901)
- Fedorov AV, Hu S, Lengaigne M, Guilyardi E (2015) The impact of westerly wind bursts and ocean initial state on the development, and diversity of El Niño events. *Clim Dyn* 44:1381–1401. doi:[10.1007/s00382-014-2126-4](https://doi.org/10.1007/s00382-014-2126-4)
- Gadgil S, Joseph PV, Joshi NV (1984) Ocean–atmosphere coupling over monsoon regions. *Nature* 312:141–143. doi:[10.1038/312141a0](https://doi.org/10.1038/312141a0)
- Gebbie G, Tziperman E (2009a) Incorporating a semi-stochastic model of ocean-modulated westerly wind bursts into an ENSO prediction model. *Theoret Appl Climatol* 97:65–73. doi:[10.1007/s00704-008-0069-6](https://doi.org/10.1007/s00704-008-0069-6)
- Gebbie G, Tziperman E (2009b) Predictability of SST-modulated westerly wind bursts. *J Clim* 22:3894–3909. doi:[10.1175/2009JCLI2516.1](https://doi.org/10.1175/2009JCLI2516.1)
- Gebbie G, Eisenman I, Wittenberg AT, Tziperman E (2007) Modulation of Westerly Wind Bursts by sea surface temperature: a semistochastic feedback for ENSO. *J Atmos Sci* 64:3281–3295. doi:[10.1175/JAS4029.1](https://doi.org/10.1175/JAS4029.1)
- Giese B, Harrison DE (1990) Aspects of the Kelvin wave response to episodic wind forcing. *J Geophys Res* 95:7289–7312. doi:[10.1029/JC095iC05p07289](https://doi.org/10.1029/JC095iC05p07289)
- Godfrey JS, Houze RA, Johnson RH, Lukas R, Redelsperger JL, Sumi A, Weller R (1998) Coupled ocean–atmosphere response experiment (COARE): an interim report. *J Geophys Res* 103:14395–14450. doi:[10.1029/97JC03120](https://doi.org/10.1029/97JC03120)
- Guilyardi E, Bellenger H, Collins M, Ferret S, Cai W, Wittenberg AT (2012) A first look at ENSO in CMIP5. *Clivar Exch* 17:29–32
- Gutzler DS (1991) Interannual fluctuations of intraseasonal variance of near-equatorial zonal winds. *J Geophys Res* 96:3173–3185. doi:[10.1029/90JD01831](https://doi.org/10.1029/90JD01831)
- Harrison DE, Giese B (1991) Episodes of surface westerly winds as observed from islands in the western tropical Pacific. *J Geophys Res* 96:3221–3237. doi:[10.1029/90JC01775](https://doi.org/10.1029/90JC01775)
- Harrison DE, Vecchi GA (1997) Westerly Wind Events in the Tropical Pacific, 1986–1995. *J Clim* 10:3131–3156. doi:[10.1175/1520-0442\(1997\)010<C3131:WWEITT>2.0.CO;2](https://doi.org/10.1175/1520-0442(1997)010<C3131:WWEITT>2.0.CO;2)
- Harrison DE, Vecchi GA (2001) El Niño and La Niña-equatorial Pacific thermocline depth and sea surface temperature anomalies, 1986–98. *Geophys Res Lett* 28:1051–1054. doi:[10.1029/1999GL011307](https://doi.org/10.1029/1999GL011307)
- Hartten L (1996) Synoptic settings of westerly wind bursts. *J Geophys Res* 101:16997–17019. doi:[10.1029/96JD00030](https://doi.org/10.1029/96JD00030)
- Hendon HH, Zhang C, Glick JD (1999) Interannual variation of the Madden–Julian oscillation during austral summer. *J Clim* 12:2538–2550. doi:[10.1175/1520-0442\(1999\)012<2538:IVOTMJ>2.0.CO;2](https://doi.org/10.1175/1520-0442(1999)012<2538:IVOTMJ>2.0.CO;2)
- Hendon HH, Wheeler M, Zhang C (2007) Seasonal dependence of the MJO-ENSO relationship. *J Clim* 20:531–543. doi:[10.1175/JCLI4003.1](https://doi.org/10.1175/JCLI4003.1)
- Hu S, Fedorov AV, Lengaigne M, Guilyardi E (2014) The impact of westerly wind bursts on the diversity and predictability of El

- Niño events: an ocean energetics perspective. *Geophys Res Lett* 41:4654–4663. doi:[10.1002/2014GL059573](https://doi.org/10.1002/2014GL059573)
- Jin FF (1997) An equatorial ocean recharge paradigm for ENSO. Part I: conceptual model Pacific. *J Atmos Sci* 54:811–829. doi:[10.1175/1520-0469\(1997\)054<0811:AEORPF>2.0.CO;2](https://doi.org/10.1175/1520-0469(1997)054<0811:AEORPF>2.0.CO;2)
- Jin FF, Lin L, Timmermann A, Zhao J (2007) Ensemble-mean dynamics of the ENSO recharge oscillator under state-dependent stochastic forcing. *Geophys Res Lett* 34:L03807. doi:[10.1029/2006GL027372](https://doi.org/10.1029/2006GL027372)
- Keen RA (1982) The role of cross-equatorial tropical cyclone pairs in the southern oscillation. *Mon Weather Rev* 110:1405–1416. doi:[10.1175/1520-0493\(1982\)110<1405:TROCTE>2.0.CO;2](https://doi.org/10.1175/1520-0493(1982)110<1405:TROCTE>2.0.CO;2)
- Kerr RA (1999) Does a globe-girdling disturbance Jigger El Niño? *Science* 285:322–323. doi:[10.1126/science.285.5426.322](https://doi.org/10.1126/science.285.5426.322)
- Kessler WS (2001) EOF representations of the Madden-Julian oscillation and its connection with ENSO. *J Clim* 14:3055–3061. doi:[10.1175/1520-0442\(2001\)014<3055:EROTMJ>2.0.CO;2](https://doi.org/10.1175/1520-0442(2001)014<3055:EROTMJ>2.0.CO;2)
- Kessler WS, Kleeman R (2000) Rectification of the Madden-Julian Oscillation into the ENSO cycle. *J Clim* 13:3560–3575. doi:[10.1175/1520-0442\(2000\)013<3560:ROTMJO>2.0.CO;2](https://doi.org/10.1175/1520-0442(2000)013<3560:ROTMJO>2.0.CO;2)
- Kessler WS, McPhaden MJ, Weickmann KM (1995) Forcing of intraseasonal Kelvin waves in the equatorial Pacific. *J Geophys Res* 100:10613–10631. doi:[10.1029/95JC00382](https://doi.org/10.1029/95JC00382)
- Kleeman R, Moore AM (1999) A new method for determining the reliability of dynamical ENSO predictions. *Mon Weather Rev* 127:694–705. doi:[10.1175/1520-0493\(1999\)127<0694:ANMFD T>2.0.CO;2](https://doi.org/10.1175/1520-0493(1999)127<0694:ANMFD T>2.0.CO;2)
- Lander MA (1990) Evolution of the Cloud Pattern during the formation of tropical cyclone twins symmetrical with respect to the Equator. *Mon Wea Rev* 118:1194–1202. doi:[10.1175/1520-0493\(1990\)118<1194:EOTCPD>2.0.CO;2](https://doi.org/10.1175/1520-0493(1990)118<1194:EOTCPD>2.0.CO;2)
- Lau KM, Peng L, Nakazawa T, Sui CH (1989) Dynamics of super cloud clusters, westerly wind bursts, 30–60 day oscillations and ENSO—An unified view. *J Meteorol Soc Jpn* 67:205–219
- Lengaigne M, Boulanger JP, Menkes C, Masson S, Madec G, Delecluse P (2002) Ocean response to the March 1997 Westerly Wind Event. *J Geophys Res* 107:8015. doi:[10.1029/2001JC000841](https://doi.org/10.1029/2001JC000841)
- Lengaigne M, Boulanger JP, Menkes C, Madec G, Delecluse P, Guilyardi E, Slingo JM (2003) The March 1997 westerly wind event and the onset of the 1997/98 El Niño: understanding the role of the atmospheric response. *J Clim* 16:3330–3343. doi:[10.1175/1520-0442\(2003\)016<3330:TMWWEA>2.0.CO;2](https://doi.org/10.1175/1520-0442(2003)016<3330:TMWWEA>2.0.CO;2)
- Lengaigne M, Boulanger JP, Delecluse P, Menkes C, Guilyardi E, Slingo JM (2004a) Westerly wind events in the Tropical Pacific and their influence on the coupled ocean-atmosphere system: a review. In: Wang C, Xie SP, Carton JA (eds) *Earth's climate*. American Geophysical Union, Washington, DC. doi:[10.1029/147GM03](https://doi.org/10.1029/147GM03)
- Lengaigne M, Guilyardi E, Boulanger JP, Menkes C, Delecluse P, Inness P, Cole J, Slingo JM (2004b) Triggering of El Niño by Westerly Wind Events in a coupled general circulation model. *Clim Dyn* 23:601–620. doi:[10.1007/s00382-004-0457-2](https://doi.org/10.1007/s00382-004-0457-2)
- Lengaigne M, Boulanger JP, Menkes C, Spencer H (2006) Influence of the seasonal cycle on the termination of El Niño events in a coupled general circulation model. *J Clim* 19:1850–1868. doi:[10.1175/JCLI3706.1](https://doi.org/10.1175/JCLI3706.1)
- Lian T, Chen D, Tang Y, Wu Q (2014) Effects of westerly wind bursts on El Niño: a new perspective. *Geophys Res Lett* 41:3522–3527. doi:[10.1002/2014GL059989](https://doi.org/10.1002/2014GL059989)
- Lin X, Johnson RH (1996) Kinematic and thermodynamic characteristics of the flow over the Western Pacific Warm Pool during TOGA COARE. *J Atmos Sci* 53:695–715. doi:[10.1175/1520-0469\(1996\)053<0695:KATCOT>2.0.CO;2](https://doi.org/10.1175/1520-0469(1996)053<0695:KATCOT>2.0.CO;2)
- Livezey RE, Chen WY (1983) Statistical field significance and its determination by Monte Carlo techniques. *Mon Weather Rev* 111:46–59. doi:[10.1175/1520-0493\(1983\)111<0046:SFSASID>2.0.CO;2](https://doi.org/10.1175/1520-0493(1983)111<0046:SFSASID>2.0.CO;2)
- Lopez H, Kirtman BP, Tziperman E, Gebbie G (2013) Impact of interactive westerly wind bursts on CCSM3. *Dyn Atmos Oceans* 59:4–51. doi:[10.1016/j.dynatmoce.2012.11.001](https://doi.org/10.1016/j.dynatmoce.2012.11.001)
- Love G (1985) Cross-equatorial interactions during tropical cyclogenesis. *Mon Weather Rev* 113:1499–1509. doi:[10.1175/1520-0493\(1985\)113<1499:CEIDTC>2.0.CO;2](https://doi.org/10.1175/1520-0493(1985)113<1499:CEIDTC>2.0.CO;2)
- Luther DS, Harrison DE, Knox RA (1983) Zonal winds in the central equatorial Pacific and El Niño. *Science* 222:327–330. doi:[10.1126/science.222.4621.327](https://doi.org/10.1126/science.222.4621.327)
- Madden RA, Julian PR (1971) Detection of a 40–50 day oscillation in the zonal wind in the Tropical Pacific. *J Atmos Sci* 28:702–708. doi:[10.1175/1520-0469\(1971\)028<0702:DOADOI>2.0.CO;2](https://doi.org/10.1175/1520-0469(1971)028<0702:DOADOI>2.0.CO;2)
- Madden RA, Julian PR (1972) Description of global-scale circulation cells in the tropics with a 40–50 day period. *J Atmos Sci* 29:1109–1123. doi:[10.1175/1520-0469\(1972\)029<1109:DOGS CC>2.0.CO;2](https://doi.org/10.1175/1520-0469(1972)029<1109:DOGS CC>2.0.CO;2)
- Madden RA, Julian PR (1994) Observations of the 40–50-day tropical oscillation—a review. *Mon Weather Rev* 122:814–837. doi:[10.1175/1520-0493\(1994\)122<0814:OOTDTO>2.0.CO;2](https://doi.org/10.1175/1520-0493(1994)122<0814:OOTDTO>2.0.CO;2)
- McPhaden MJ (1999) Genesis and evolution of the 1997–1998 El Niño. *Science* 283:950–954. doi:[10.1126/science.283.5404.950](https://doi.org/10.1126/science.283.5404.950)
- McPhaden MJ (2002) Mixed layer temperature balance on intraseasonal timescales in the equatorial Pacific Ocean. *J Clim* 15:2632–2647. doi:[10.1175/1520-0442\(2002\)015<2632:MLTB OI>2.0.CO;2](https://doi.org/10.1175/1520-0442(2002)015<2632:MLTB OI>2.0.CO;2)
- McPhaden MJ (2004) Evolution of the 2002/03 El Niño. *Bull Am Meteorol Soc* 85:677–695. doi:[10.1175/BAMS-85-5-677](https://doi.org/10.1175/BAMS-85-5-677)
- McPhaden MJ, Taft BA (1988) Dynamics of seasonal and intraseasonal variability in the Eastern Equatorial Pacific. *J Phys Oceanogr* 18:1713–1732. doi:[10.1175/1520-0485\(1988\)018<1713:DOSAI V>2.0.CO;2](https://doi.org/10.1175/1520-0485(1988)018<1713:DOSAI V>2.0.CO;2)
- McPhaden MJ, Yu X (1999) Equatorial waves and the 1997–98 El Niño. *Geophys Res Lett* 26:2961–2964. doi:[10.1029/1999JGL004901](https://doi.org/10.1029/1999JGL004901)
- McPhaden MJ, Zebiak SE, Glantz MH (2006a) ENSO as an integrating concept in earth science. *Science* 314:1740–1745. doi:[10.1126/science.1132588](https://doi.org/10.1126/science.1132588)
- McPhaden MJ, Zhang X, Hendon HH, Wheeler M (2006b) Large scale dynamics and MJO forcing of ENSO variability. *Geophys Res Lett* 33:L16702. doi:[10.1029/2006GL026786](https://doi.org/10.1029/2006GL026786)
- Meinen C, McPhaden MJ (2000) Observations of warm water volume changes in the equatorial Pacific and their relationship to El Niño and La Niña. *J Clim* 13:3551–3559. doi:[10.1175/1520-0442\(2000\)013<3551:Oowwvc>2.0.Co;2](https://doi.org/10.1175/1520-0442(2000)013<3551:Oowwvc>2.0.Co;2)
- Menkes C, Lengaigne M, Vialard J, Puy M, Marchesiello P, Cravatte S, Cambon G (2014) About the role of Westerly Wind Events in the possible development of an El Niño in 2014. *Geophys Res Lett* 41(6476):6483. doi:[10.1002/2014GL061186](https://doi.org/10.1002/2014GL061186)
- Nitta T (1989) Development of a twin cyclone and westerly bursts during the initial phase of the 1986–1987 El Niño. *J Meteorol Soc Japan* 67:677–681
- Perez CL, Moore AM, Zavala-Garay J, Kleeman R (2005) A comparison of the influence of additive and multiplicative stochastic forcing on a coupled model of ENSO. *J Clim* 18:5066–5085. doi:[10.1175/JCLI3596.1](https://doi.org/10.1175/JCLI3596.1)
- Perigaud C, Cassou C (2000) Importance of oceanic decadal trends and westerly wind bursts for forecasting El Niño. *Geophys Res Lett* 27:389–392. doi:[10.1029/1999GL010781](https://doi.org/10.1029/1999GL010781)
- Praveen Kumar B, Vialard J, Lengaigne M, Murty VSN, McPhaden MJ, Cronin MF, Pinsard F, Gopala Reddy K (2012) TropFlux wind stresses over the tropical oceans: evaluation and comparison with other products. *Clim Dyn* 40:2049–2071. doi:[10.1007/s00382-012-1455-4](https://doi.org/10.1007/s00382-012-1455-4)

- Rashid HA, Hendon HH, Wheeler M, Alves O (2010) Prediction of the Madden–Julian oscillation with the POAMA dynamical prediction system. *Clim Dyn* 36:649–661. doi:[10.1007/s00382-010-0754-x](https://doi.org/10.1007/s00382-010-0754-x)
- Roulston MS, Neelin JD (2000) The response of an ENSO model to climate noise, weather noise and intraseasonal forcing. *Geophys Res Lett* 27:3723–3726. doi:[10.1029/2000GL011941](https://doi.org/10.1029/2000GL011941)
- Rui H, Wang B (1990) Development characteristics and dynamic structure of tropical intraseasonal convection anomalies. *J Atmos Sci* 47:357–379. doi:[10.1175/1520-0469\(1990\)047<0357:DCA DSO>2.0.CO;2](https://doi.org/10.1175/1520-0469(1990)047<0357:DCA DSO>2.0.CO;2)
- Seiki A, Takayabu YN (2007a) Westerly wind bursts and their relationship with intraseasonal variations and ENSO. Part I: statistics. *Mon Weather Rev* 135:3325–3345. doi:[10.1175/MWR3477.1](https://doi.org/10.1175/MWR3477.1)
- Seiki A, Takayabu YN (2007b) Westerly wind bursts and their relationship with intraseasonal variations and ENSO. Part II: energetics over the Western and Central Pacific. *Mon Wea Rev* 135:3346–3361. doi:[10.1175/MWR3477.1](https://doi.org/10.1175/MWR3477.1)
- Shi L, Alves O, Hendon HH (2009) The role of stochastic forcing in ensemble forecasts of the 1997/98 El Niño. *J Clim* 22:2526–2540. doi:[10.1175/2008JCLI2469.1](https://doi.org/10.1175/2008JCLI2469.1)
- Sui CH, Lau KM (1992) Multiscale phenomena in the Tropical Atmosphere over the Western Pacific. *Mon Weather Rev* 120:407–430. doi:[10.1175/1520-0493\(1992\)120<0407:MPITTA>2.0.CO;2](https://doi.org/10.1175/1520-0493(1992)120<0407:MPITTA>2.0.CO;2)
- Trenberth KE, Large WG, Olson JG (1989) The effective drag coefficient for evaluating wind stress over the oceans. *J Clim* 2:1507–1516. doi:[10.1175/1520-0442\(1989\)002<1507:TEDCFE>2.0.CO;2](https://doi.org/10.1175/1520-0442(1989)002<1507:TEDCFE>2.0.CO;2)
- Trenberth KE, Branstator GW, Karoly D, Kuma A, Lau KM, Ropelewski C (1998) Progress during TOGA in understanding and modeling global teleconnections associated with tropical sea surface temperatures. *J Geophys Res* 103:14291. doi:[10.1029/97JC01444](https://doi.org/10.1029/97JC01444)
- Tziperman E, Yu L (2007) Quantifying the dependence of westerly wind bursts on the large-scale tropical pacific SST. *J Clim* 20:2760–2768. doi:[10.1175/JCLI4138a.1](https://doi.org/10.1175/JCLI4138a.1)
- Van Oldenborgh GJ (2000) What caused the onset of the 1997–98 El Niño? *Mon Weather Rev* 128:2601–2607. doi:[10.1175/1520-0493\(2000\)128<2601:WCTOOT>2.0.CO;2](https://doi.org/10.1175/1520-0493(2000)128<2601:WCTOOT>2.0.CO;2)
- Vecchi GA, Harrison DE (2000) Tropical Pacific sea surface temperature anomalies, El Niño, and equatorial westerly wind events. *J Clim* 13:1814–1830. doi:[10.1175/1520-0442\(2000\)013<1814:TPSSTA>2.0.CO;2](https://doi.org/10.1175/1520-0442(2000)013<1814:TPSSTA>2.0.CO;2)
- Vecchi GA, Wittenberg AT (2010) El Niño and our future climate: where do we stand? *Wiley Interdiscip Rev Clim Change* 1:260–270. doi:[10.1002/wcc.33](https://doi.org/10.1002/wcc.33)
- Vecchi GA, Wittenberg AT, Rosati A (2006) Reassessing the role of stochastic forcing in the 1997–1998 El Niño. *Geophys Res Lett* 33:L01706. doi:[10.1029/2005GL024738](https://doi.org/10.1029/2005GL024738)
- Verbickas S (1998) Westerly wind bursts in the tropical Pacific. *Weather* 53:282–284. doi:[10.1002/j.1477-8696.1998.tb06401.x](https://doi.org/10.1002/j.1477-8696.1998.tb06401.x)
- Wang W, Chen M, Kumar A, Xue Y (2011) How important is intraseasonal surface wind variability to real-time ENSO prediction? *Geophys Res Lett* 38:L13705. doi:[10.1029/2011GL047684](https://doi.org/10.1029/2011GL047684)
- Wheeler M, Hendon HH (2004) An All-season real-time multivariate MJO Index: development of an Index for monitoring and prediction. *Mon Weather Rev* 132:1917–1932. doi:[10.1175/1520-0493\(2004\)132<1917:AARMMI>2.0.CO;2](https://doi.org/10.1175/1520-0493(2004)132<1917:AARMMI>2.0.CO;2)
- Wheeler M, Kiladis GN (1999) Convectively coupled equatorial waves: analysis of clouds and temperature in the wavenumber-frequency domain. *J Atmos Sci* 56:374–399. doi:[10.1175/1520-0469\(1999\)056<0374:CCEWAO>2.0.CO;2](https://doi.org/10.1175/1520-0469(1999)056<0374:CCEWAO>2.0.CO;2)
- Yang GY, Hoskins B, Slingo JM (2007) Convectively coupled equatorial waves. Part I: horizontal and vertical structures. *J Atmos Sci* 64:3406–3423. doi:[10.1175/JAS4017.1](https://doi.org/10.1175/JAS4017.1)
- Yu X, McPhaden MJ (1999) Seasonal variability in the Equatorial Pacific. *J Phys Oceanogr* 29:925–947. doi:[10.1175/1520-0485\(1999\)029<0925:SVITEP>2.0.CO;2](https://doi.org/10.1175/1520-0485(1999)029<0925:SVITEP>2.0.CO;2)
- Yu L, Rienecker MM (1998) Evidence of an extratropical atmospheric influence during the onset of the 1997–98 El Niño. *Geophys Res Lett* 25(18):3537–3540. doi:[10.1029/98GL02628](https://doi.org/10.1029/98GL02628)
- Zavala-Garay J, Zhang C, Moore AM, Kleeman R (2005) The linear response of ENSO to the Madden–Julian oscillation. *J Clim* 18:2441–2459. doi:[10.1175/JCLI3408.1](https://doi.org/10.1175/JCLI3408.1)
- Zhang C (1996) Atmospheric intraseasonal variability at the surface in the Tropical Western Pacific Ocean. *J Atmos Sci* 53:739–758. doi:[10.1175/1520-0469\(1996\)053<0739:AIVATS>2.0.CO;2](https://doi.org/10.1175/1520-0469(1996)053<0739:AIVATS>2.0.CO;2)
- Zhang C (2005) Madden–Julian oscillation. *Rev Geophys* 43:RG2003. doi:[10.1029/2004RG000158](https://doi.org/10.1029/2004RG000158)
- Zhang C, Gottschalck J (2002) SST anomalies of ENSO and the Madden–Julian oscillation in the equatorial Pacific. *J Clim* 15:2429–2445. doi:[10.1175/1520-0442\(2002\)015<2429:SAOEAT>2.0.CO;2](https://doi.org/10.1175/1520-0442(2002)015<2429:SAOEAT>2.0.CO;2)